AMER. ZOOL., 40:597–630 (2000)

Calculating Climate Effects on Birds and Mammals: Impacts on Biodiversity, Conservation, Population Parameters, and Global Community Structure[1]

WARREN P. PORTER,[2,*] SRINIVAS BUDARAJU,[3,†] WARREN E. STEWART,† AND NAVIN RAMANKUTTY‡

**Department of Zoology, University of Wisconsin, 250 N. Mills St., Madison, Wisconsin 53706*
†Department of Chemical Engineering, University of Wisconsin, 1415 Johnson Drive, Madison, Wisconsin 53706
‡Institute for Environmental Studies, 1225 West Dayton Street, Madison, Wisconsin 53706

SYNOPSIS. This paper describes how climate variation in time and space can constrain community structure on a global scale. We explore body size scaling and the energetic consequences in terms of absorbed mass and energy and expended mass and energy. We explain how morphology, specific physiological properties, and temperature dependent behaviors are key variables that link individual energetics to population dynamics and community structure.

This paper describes an integrated basic principles model for mammal energetics and extends the model to bird energetics. The model additions include molar balance models for the lungs and gut. The gut model couples food ingested to respiratory gas exchanges and evaporative water loss from the respiratory system. We incorporate a novel thermoregulatory model that yields metabolic calculations as a function of temperature. The calculations mimic empirical data without regression. We explore the differences in the quality of insulation between hair and feathers with our porous media model for insulation.

For mammals ranging in size from mice to elephants we show that calculated metabolic costs are in agreement with experimental data. We also demonstrate how we can do the same for birds ranging in size from hummingbirds to ostriches. We show the impact of changing posture and changing air temperatures on energetic costs for birds and mammals. We demonstrate how optimal body size that maximizes the potential for growth and reproduction changes with changing climatic conditions and with diet quality. Climate and diet may play important roles in constraining community structure (collection of functional types of different body sizes) at local and global scales. Thus, multiple functional types may coexist in a locality in part because of the temporal and spatial variation in climate and seasonal food variation. We illustrate how the models can be applied in a conservation and biodiversity context to a rare and endangered species of parrot, the Orange-bellied Parrot of Australia and Tasmania.

INTRODUCTION

A brief history

Ever since the era of Charles Darwin biologists have been intrigued by how and why animals live where they do and what is it about their properties that makes them appear where they do, and appear in the species associations that they form. Hutchinson (1959) defined the concept of the niche. MacArthur *et al.* (1966), Roughgarden (1974) and many others explored aspects of how size and habitat may influence community structure. Norris (1967) and Bartlett and Gates (1967) were the first to calculate explicitly how climate affects animal heat and mass balance and the consequences for body temperature in outdoor

[1] From the Symposium *Evolutionary Origin of Feathers* presented at the Annual Meeting of the Society for Integrative and Comparative Biology, 6–10 January 1999, at Denver, Colorado.

[2] E-mail: wporter@mhub.zoology.wisc.edu

[3] Current address: West Vaco Laurel Research Laboratory, 11101 John's Hopkins Road Laurel, MD 20723.

environments. The climate space concept emerged from steady state heat and mass balance calculations and was used to explore how climates might constrain animal survival outdoors (Porter and Gates, 1969).

Those early animal models of the 1960s were limited by the lack of models for distributed heat generation internally, distributed evaporative water loss internally, and a first principles model of gut function. Batch reactor, plug flow and other models were already in existence in the chemical engineering literature (Bird *et al.*, 1960) and it would take time for the biological community to rediscover them. Also missing were a first principles model of porous insulation for fur or feathers, an appendage model, and a general microclimate model that could use local macroclimate data to calculate the range of local microenvironments above and below ground. It became possible to estimate convection heat transfer properties knowing only the volume of an animal (Mitchell, 1976). Another useful development was the appearance of a countercurrent heat exchange model for appendages (Mitchell and Myers, 1968) and the measurement of heat transfer characteristics from animal appendage shapes (Wathen *et al.*, 1971, 1974). It also became possible to deal with outdoor turbulence effects on convective heat transport (Kowalski and Mitchell, 1976). A general-purpose microclimate model emerged in the early 1970s (Beckman *et al.*, 1971; Porter *et al.*, 1973; Mitchell *et al.*, 1975) that calculated above and below ground microclimates. The ability to deal with local environmental heterogeneity and calculate percent of thermally available habitat came later (Grant and Porter, 1992). Over time general-purpose conduction–radiation porous media models for fur appeared in the biological literature (Kowalski, 1978) and it became possible to refine and test them in a variety of habitats and on many species (Porter *et al.*, 1994). The extension of the models to radial instead of Cartesian coordinates and the implementation of first principles fluid mechanics in the porous media (Stewart *et al.*, 1993; Budaraju *et al.*, 1994, 1997) added important new dimensions to the models, which could now calculate temperature and velocity profiles and therefore heat and mass transfer within the fur from basic principles. A test of the ectotherm and microclimate models to estimate a species' survivorship, growth and reproduction at a continental scale appeared in the mid 1990s (Adolph and Porter, 1993, 1996).

Thanks to these developments and the ones reported in this paper, such as the temperature dependent behavior linked to the new thermoregulatory model, it is now possible to ask: ''How does climate affect individual animals' temperature dependent behavior and physiology and what role(s) does it play in population dynamics and community structure?'' This paper attempts to address some of these questions.

We approach the problem from the perspective of a combination of heat and mass transfer engineering and specific aspects of morphology, physiology and temperature dependent behavior of individuals. We show how this interactive combination is essential to calculate *preferred activity time* that *minimizes size specific heat/water stress.*

Preferred activity time is a key link between individual energetics and population level variables of survivorship, growth and reproduction, since it impacts all three population variables. Both individual and population level effects may place constraints on community structure. At the *individual level,* climate at any given time and food type and quality affect the optimal body size that maximizes discretionary mass and energy, the resources needed for growth and reproduction. Climate also affects community structure by affecting individual survivorship directly (heat balance/metabolic costs) and indirectly (activity time overlap of predator and prey). Climate affects seasonal food availability, distribution of food in space and time, and the cost of foraging for that food at different times during a day. Survivorship is affected by temperature dependent behavior changes that allow animals to move to less costly microenvironments at any time. For small mammals, underground burrows or under snow tunnels provide temperatures that never stay below 0°C due to local heating effects of the animal's metabolic heat production.

At the *population level*, climate plays a very important role in population numbers. Each species interacts in its own way with climate, affecting its abundance, and community structure. As Ives *et al.* (1999 p. 546) have pointed out

> Our main result is that interspecific competition and species number have little influence on community-level variances; the *variance in total community biomass depends only on how species respond to environmental fluctuations*. This contrasts with arguments (Tilman and Downing, 1994; Lawton and Brown, 1993) that interspecific competition may decrease community-level variances by driving negative covariances between species abundances. We show that negative covariances are counteracted by increased species-level variances created by interspecific competition.
>
> Consequently, assessing the effect of biodiversity on community variability should emphasize species-environment interactions and differences in species' sensitivities to environmental fluctuations (for example, drought-tolerant species and phosphorus-limited species) (McNaughton, 1977, 1985; Frost *et al.*, 1994). Competitive interactions are relatively unimportant except through their effects on mean abundances. We have focused on competitive communities, because much current experimental work has addressed competition among plants. Nonetheless, the same results can be shown to hold for more complex models with multiple trophic levels.

Exactly how climate variation, vegetation differences, animal morphology, and foraging behavior all interact to constrain multiple functional types' existence as a community is still largely unknown. Very little is known about temperature dependent foraging in mammals, although this has been well studied in reptiles and insects. Quantitative consequences of functional morphology on encounter probability and food handling time also are relatively unexplored as yet in mammals.

Temporal climate variation in a locality creates the opportunity for multiple optimal body sizes over annual cycles. The *spatial* local variation in topography and vegetation creates multiple local climates. Thus temporal and spatial variation in climate creates opportunities for multiple functional types (sizes) to coexist as communities, because as we shall see below, different body sizes interact differently with climate. Qualitatively, this idea is not new. However with likely major shifts in global climates and the rapid global changes in land use, there is urgent need to move these qualitative ideas to a quantitative framework for protection of biodiversity, conservation biology, and a number of other applications. We focus in this paper on applications to mammals and birds.

An overview of this paper

The structure of the paper begins with an overview of how macroclimate drives microclimates, which in turn impact individual animal properties. We then show how key individual properties determine population level parameters that can be used to calculate population dynamics variables. We then illustrate how individual properties also impact on community structure, that in turn feed back to temperature dependent animal properties of individuals.

The initial overview provides a context for an analysis of the model components and their interactions in hierarchical contexts. We start with the model components from the core to the skin, then from the skin through the insulation to the environment. We demonstrate how these components collectively can define the metabolic cost to mammals ranging in size from mice to elephants. We show how the empirical mouse-to-elephant metabolic regression line for animals of different sizes changes depending upon the animal's climate and posture.

Then we explore how changing mammal body size affects discretionary energy across all climates. Once the mammal model is explored, we repeat the process for the bird model. We demonstrate how we can estimate metabolic cost across bird sizes ranging from hummingbirds to ostriches. We show how postural changes and air tem-

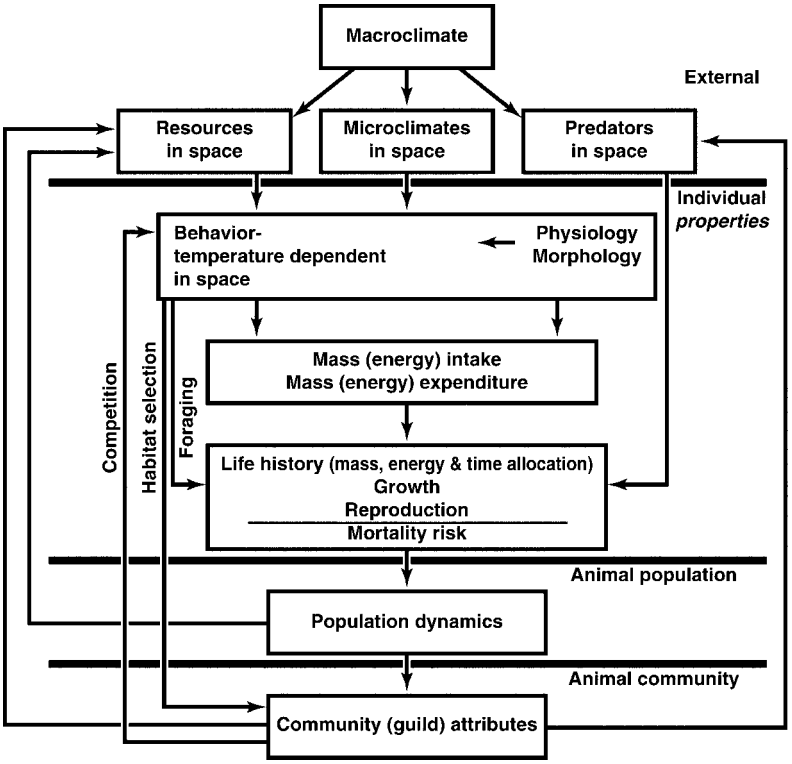

FIG. 1. Flow diagram illustrating the interconnections between climate, individual properties, population dynamics, and community structure.

perature can alter metabolic cost estimates for birds.

Once sensitivity analyses are completed, we explore how temporal and spatial variation in global climate impact body size dependent discretionary energy assuming no food limitation and thereby place constraints on the potential combinations of body sizes (community structure) of mammals at the global scale.

Finally, we show how these models can be applied to estimate for the first time from basic principles the metabolic costs and food requirements of an endangered species of bird, the Orange-bellied Parrot of Tasmania and Australia. We show these results for body sizes ranging from hatchling to fully mature adult for a wide range of environmental conditions.

MATERIALS AND METHODS

The models

Overview. Figure 1 is a flow diagram that shows qualitatively how we connect macroclimate, microclimates, individual properties, population level effects, and community attributes. The *macroclimate–microclimate connection* is achieved in part by general climate data available through the National Oceanic and Atmospheric Administration (NOAA). The microclimate model has been described for a variety of habitats that range from southwestern deserts (Mitchell *et al.*, 1975; Porter *et al.*, 1973) to Santa Fe Island in the Galapagos (Christian *et al.*, 1983) to Michigan bogs (Kingsolver, 1979). It is a one-dimensional finite difference model that simultaneously solves the heat and mass balance equations for the ground surface and below. It also calculates wind speed and temperature profiles from the ground surface to two meter reference height, where meteorological data are typically measured. Clear sky solar radiation is calculated from basic principles (McCullough and Porter, 1971).

Microclimate calculations for heteroge-

neous environments can determine percent of thermally available habitat and temperature dependent feeding frequency (Grant and Porter, 1992). Grant and Porter showed that *item feeding frequency was a linear function of the thermally available percent of the habitat* (the percentage that allows the animal to stay within its preferred temperature range, thereby avoiding significant thermoregulatory heat stress costs). A summation of a day's preferred activity times over a month and over the year yields total annual activity time.

Total annual activity time is a key variable linking individual energetics with population and community level phenomena. Annual activity time for a terrestrial vertebrate was first calculated from basic principles in 1973 (Porter *et al.*, 1973). By ''basic principles'' we mean equations derived from thermodynamic principles that do not involve regression equations. Total annual activity time can be used to calculate key life history variables, such as survivorship, growth, and reproductive potential (Adolph and Porter, 1993; Adolph and Porter, 1996), that are used to calculate population dynamics.

Survivorship (mortality) probability/hour is affected by activity time, which is affected by temperature dependent habitat selection. Climate change may affect survivorship, partly by modifying predation probabilities that change with seasonal changes in overlap of predator and prey preferred activity time (Porter *et al.*, 1973; Porter and James, 1979) and partly due to climate stress (Porter and Gates, 1969).

Growth and reproduction potential depend on mass and energy intake and expenditures. The difference between intake and expenditure is the capital available for growth or reproduction. We are in a strong position to calculate mass/energy expenditures. Intake of mass and energy is more challenging. Intake depends on item feeding frequency and handling time. Handling time depends on the size of food ''packages'' and morphology of the feeding apparatus. Calculations in this paper assumed no shortage of food and that the mass flow through the gut scales with mass (Calder, 1984) and meets the body size/climate imposed metabolic demand. The mass flow absorbed over a day is assumed sufficient to meet basic thermoregulatory requirements for the day plus a user defined multiplier (up to 7) above the minimal metabolism needed to maintain core temperature in the current climate. This was done to try to establish an *upper bound* for absorbed mass for different sizes of animals.

Different sizes of animals may represent different trophic levels in the community Only some of the connections between a species' individual energetics, population dynamics and community attributes are shown in Figure 1. Other species within the habitat may influence temperature dependent behavior by competing with the arbitrarily chosen animal species represented here, thereby affecting their numbers (Ives *et al*., 1999). The reader may imagine multiple layers of this graph for individual species interconnected vertically to allow for explicit multiple species descriptions.

Model cross section

Figure 2 represents a diagrammatic cross section through an arbitrarily chosen part of an animal. This could represent a torso whose geometry may be approximated by a cylinder, sphere, or ellipsoid, or even a cross section through an appendage, if the heat loss by respiration is removed. There may or may not be a porous insulation beyond the skin. Figure 2 shows what would be needed for heat and mass transfer calculations. Data needed are the mean length of the fibers (hair or hair-like elements in feathers), fiber density as a function of depth, fiber diameter, and the depth of the insulation. Length and depth of the fibers are usually different unless the fibers extend outward normal to the skin. Solar reflectivity and transmissivity of the fibers also must be known if the animal is diurnal and exposed to sunlight. The environmental conditions that specify the climate boundary conditions for an individual include solar radiation, infrared fluxes from the sky and ground, air temperature, wind speed, and relative humidity of the air passing over the animal. These values are calculated based on the animal's average height above

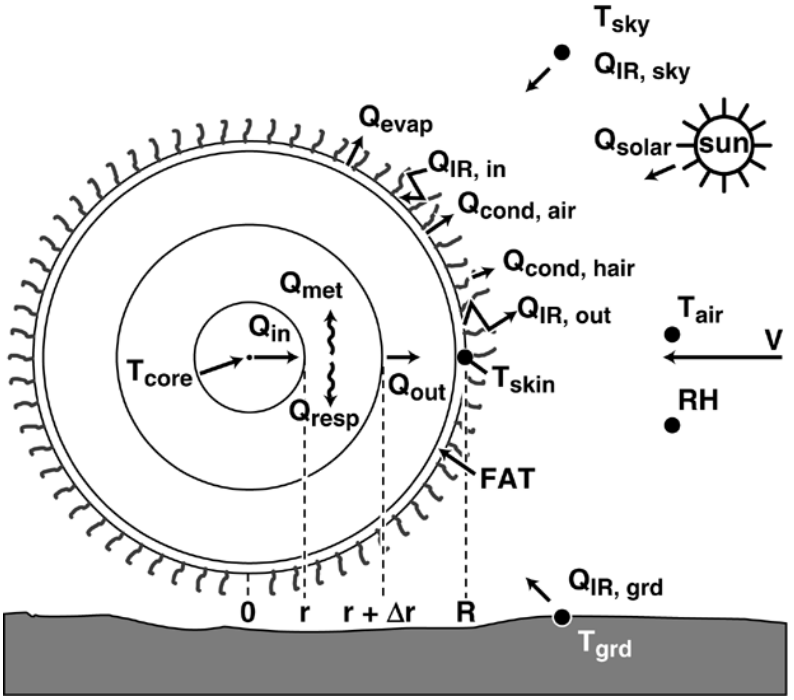

FIG. 2. Diagram of a cross-section of an animal with porous insulation and heat fluxes including uniform heat generation and uniform heat dissipation by respiration. See abbreviations list for definitions of terms.

ground and the microclimate calculations for environment conditions above ground. The microclimate equations have been described (Mitchell *et al.,* 1975; Porter *et al.,* 1973).

Most of the equations describing *porous media* heat flux without convection through the fur are described (Conley and Porter, 1986; Porter *et al.,* 1994). Heat and mass flux equations describing flow through fur are complex (Stewart *et al.,* 1993; Budaraju *et al.,* 1994, 1997). Solar radiation was incorporated in the model used here by *assuming that solar radiation is absorbed very close to the fur/feather–air interface,* which is usually the case for bird feathers and dark, dense fur (Porter, unpublished data). Absorbed solar radiation heats the fiber elements, which then emit infrared radiation outward toward the sky and inward through the porous insulation. The watts of *absorbed* solar radiation were treated as an additional source of thermal radiation from the sky for the half of the animal exposed to the sky. Thus, the diffuse infrared radiation equations already in model were also used for incorporating absorbed solar radiation in the model.

The porous media model is only part of the animal model used to calculate metabolic heat production that will maintain core temperature given the internal and external morphology of the animal, including its insulation (Porter *et al.,* 1994). The radial dimension of an animal is calculated from its weight and geometry. An iterative searching routine named Zbrent guesses the metabolic heat production needed to maintain any specified core temperature (Press *et al.,* 1986). Zbrent finds the unique metabolic heat production that satisfies the heat and mass balance equations (Appendix, Porter *et al.,* 1994) given the body allometry, dimensions, specified core temperature, insulation properties, and environmental conditions. Because the equations are interconnected, relatively few variables determine these solutions (Porter *et al.,* 1994).

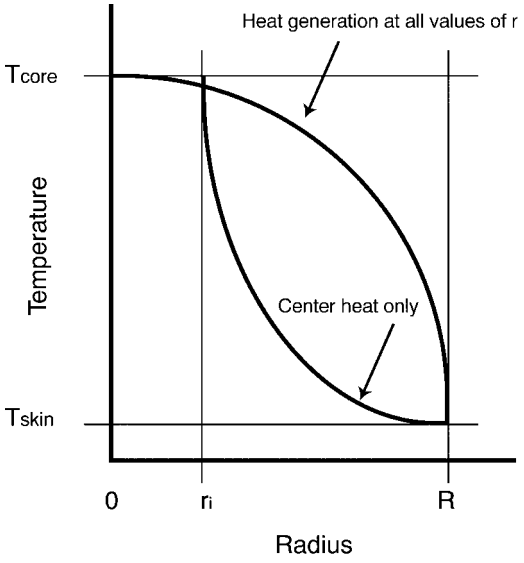

FIG. 3. Temperature profiles in the body for models of uniform heat generation vs. heat generation in a central region with radial conduction only.

Inside the body

The type of food in the gut determines the relative proportions of carbohydrates, proteins and lipids that are absorbed by the body. A healthy body will utilize these absorbed molecules as substrates. The demand for energy and the substrates being oxidized determine the amount of oxygen needed. The oxygen consumption is associated with heat generation. The proportion of the substrates oxidized determines the amount of carbon dioxide produced and hence the respiratory quotient. The oxygen demand specifies the moles of air that must pass through the respiratory system to meet the demand. Thus, the type of food in the gut affects indirectly the amount of incoming respiratory air, which in turn affects the water balance in the respiratory system in the heat generation-ventilation-gut coupled model described below.

Heat generation models. Figure 3 shows how the *current model* of distributed heat generation throughout the body creates a parabolic temperature profile from the body core to skin. The equations describing uniform heat generation for rectangular (slab), cylindrical, spherical, and ellipsoid geometry (Porter *et al.,* 1994) all show that the internal heat generation and the temperature gradient from core to skin are functions of the body radius squared. The model solves the heat and mass balance equations (Porter *et al.,* 1994) for heat generation needed to maintain core temperature by iterative guessing the solution for each hour of simulation throughout a 24 hr daily cycle. The coupled equations of heat and mass transfer simultaneously yield solutions for water balance, gut absorbed food requirements, hours of activity time and discretionary mass and energy available for growth or reproduction or fat deposition as described below.

Earlier metabolic heat generation models, such as a slab approximation, assumed a heat source only at the center of the animal (Porter and Gates, 1969; Porter *et al.,* 1973). This assumption creates a simple linear temperature profile from core to skin (Fig. 3, Porter *et al.,* 1994), but not shown here. This type of construct frequently uses the term ''thermal conductance,'' the reciprocal of'' thermal resistance.'' Thermal conductance is a linear model of heat transfer commonly used in many biological publications referring to animal heat transfer. Unfortunately it is only relevant in the context of non-heat generating materials.

A cylindrical geometry with a heat source only at the center (*axis*) does not mathematically allow for the heat source only at the axis, since it is undefined there (Bird *et al.,* 1960). A central heated *region* is required. Simple conduction (but not added heat generation by the conducting tissues) of heat radially from the perimeter of the core region yields a logarithmic temperature profile. This logarithmic profile has different heat generation requirements to maintain a specified core temperature in the center region than a model using distributed heat production from the core to the skin.

Respiration. An important *addition to the current model* is the distributed respiratory water loss, which represents lungs that span most of the body cavity. This innovation gives much better agreement of predicted metabolic rates with measured values.

Figure 4 shows the system diagram for the lung molar balance model. A dashed

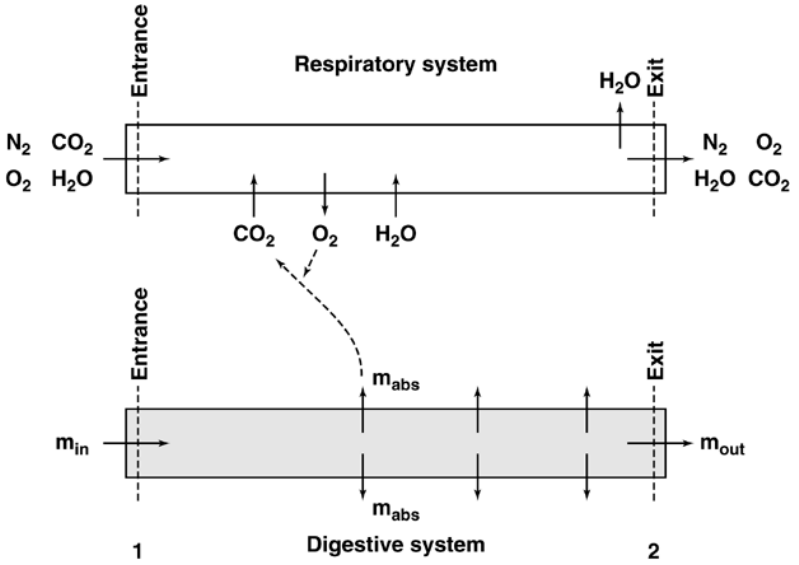

FIG. 4. Molar balance models of respiratory and digestive systems coupled to each other and to (oxygen requirement for) metabolic heat demand to maintain core temperature.

line labeled 1 represents the entrance surface to the respiratory system. The dashed line labeled 2 represents the exit surface from the respiratory system. Moles of nitrogen, oxygen, water, and carbon dioxide enter the respiratory system. The moles of air entering are calculated from the product of the moles of oxygen needed for the current guess for heat generation requirements times the sum of the percent composition of the components of air divided by the percent of oxygen in the air, which may change in burrows. Thus, the current iterative guess for metabolic heat production specifies how many moles of oxygen are needed to meet the metabolic demand from the respiratory system. The type of diet (carbohydrate/protein/lipid) specifies the joules of heat produced from the oxidation of a mole of oxygen (Schmidt-Nielsen, 1979). The oxygen extraction efficiency of the respiratory system and the properties of air determine how many moles of air are needed per unit time by the respiratory system. The amount of carbon dioxide added to the respiratory system air is calculated from the respiratory quotient, RQ, which is the ratio of moles of carbon dioxide produced per mole of oxygen consumed (Schmidt-Nielsen, 1979).

The RQ changes with different substrates oxidized. The respiration model uses the RQ for carbohydrates, proteins, or lipids, or a combination of the three, to calculate the amount of carbon dioxide that flows out of the respiratory surfaces. The user-specified proportions of carbohydrate, protein, and lipid in the food consumed thus ultimately determine the RQ. Thus, the metabolic oxygen demand to maintain core temperature and the current properties of air specify the volume of airflow and the amount of water added to saturate the respiratory system air. At expiration, the user specified temperature difference between the air in contact with nasal surfaces as air exits at surface 2 and the free stream external air (1–3°C) is used to calculate the amount of water recovered by condensation on the nasal surfaces. The calculated skin temperature of the body would not be relevant for estimating nasal air temperature at exit because of the different convective environment inside the nares *vs.* the outer skin covered with fur or feathers. Since we were trying to estimate maximum recovery rates as an upper bound, we used experimental data summarized from the literature (Welch, 1980) for the calculations and used a 3°C

difference between exit air temperature and local external (free stream) air temperature.

Temperature regulation model. Another important *addition to the model* was temperature regulation responses. Sensitivity analyses of the model done by increasing air and radiation temperatures revealed that the calculated skin temperature, which is a function of the specified core temperature, must not exceed core temperature. If it does exceed the core temperature, metabolic heat production must be dissipated by evaporation of respiratory water to achieve steady state. The molar balance model for the lungs just described clearly showed a limited capacity for heat dissipation by water vaporization in the lungs, which is consistent with experimental data (Welch and Tracy, 1977; Welch, 1980). A user specified minimum core–skin temperature difference was added to the model. The value used in our calculations was 0.5°C. If an iterative solution for heat generation given the specified core temperature produced a skin temperature less than the minimum core–skin difference, a three-level hierarchy of physiological responses was invoked.

First, flesh thermal conductivity increases to the maximum value measured in the literature. That was never sufficient to increase the core-skin temperature gradient, since it only serves to increase skin temperature.

Second, the percentage of the skin surface assumed covered with tiny water drops increases up to 100 percent of the skin surface area to cool the skin. The amount of cooling is constrained by air temperature, wind speed, relative humidity, and the boundary layer thickness at the skin. The latter is a function of body characteristic dimension, insulation properties, and wind properties defined in Nusselt and Reynolds numbers (Bird *et al.,* 1960). The Nusselt number is simply a nondimensional ratio of the heat transfer coefficient times a characteristic dimension (often defined as the distance a fluid such as air travels when passing over the object of interest) divided by the thermal conductivity of the fluid. The Reynolds number is also a nondimensional ratio. It is the product of the fluid density, velocity, and the characteristic dimension divided by the dynamic viscosity of the fluid. The Nusselt number is often plotted against the Reynolds number. The regression of the data plotted is a relationship that allows for the calculation of the heat transfer coefficient (used to calculate convective heat loss) for any value of Reynolds numbers variables, such as changing characteristic dimension (body size).

Third, failing all else, the core temperature is allowed to rise in 0.1°C increments until a stable solution of the equation is found that allows a 0.5°C temperature difference between core and skin. This approach causes a rise in metabolic rate at high temperatures that is observed experimentally (Schmidt-Nielsen, 1979). It also mimics the rise in core temperature that is observed experimentally (Schmidt-Nielsen, 1979). No regressions are needed to emulate the experimental data.

The gut. Figure 4 also shows the system diagram for the molar balance gut model. It is related to the well-known batch reactor and plug flow model originally developed in chemical engineering and subsequently applied to animal digestive systems (Penry and Jumars, 1987). The model used here allows for any type of ingested food consisting of user specified proportions of carbohydrates, lipids, proteins and water content. The food can enter the gut any time during activity time in any amount, subject to the constraint that the volume of food ingested per day may not exceed the wet mass of the animal. The energy value of absorbed carbohydrates, lipids, and proteins is well known (Schmidt-Nielsen, 1979). Details of the model are in the Appendix.

Temperature dependent feeding. Figure 5 shows how these animal models respond to different temperatures. The metabolic rate of an endotherm changes with increasing environmental temperature in a distorted U-shaped curve (Bucher *et al.,* 1986; Kleiber, 1975; Morris and Kendeigh, 1981; Schmidt-Nielsen, 1979; Scholander, 1940). It is commonly assumed from a physiological perspective that the capacity to absorb food is independent of environmental temperature because of the relatively constant

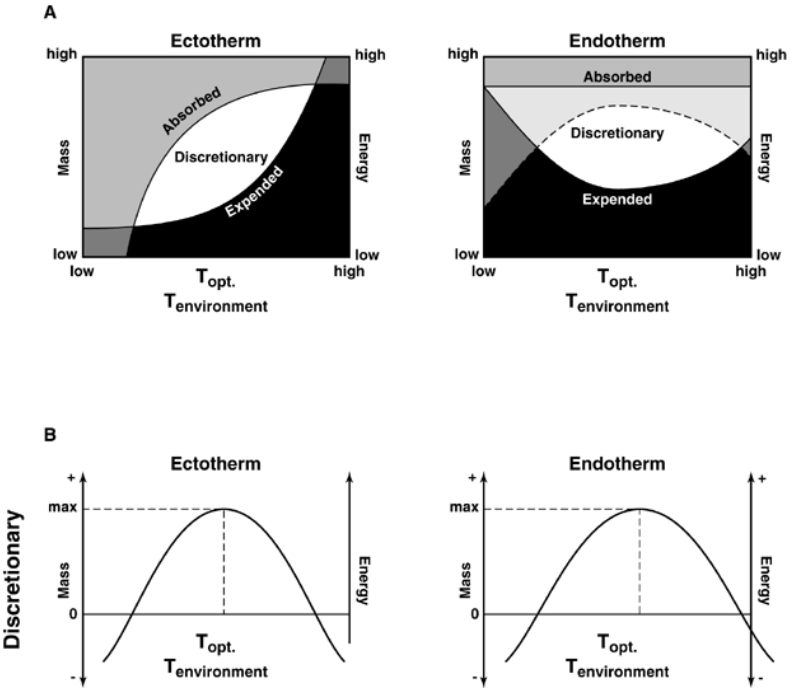

FIG. 5. A qualitative comparison between intake and expenditure of mass and energy as a function of environmental temperature for ectotherms and endotherms. In ectotherms, mass absorbed depends upon temperature dependent digestion physiology, which typically ceases at temperatures below 15–20°C. Discretionary energy uptake (fitness measure) is a function of environmental temperature because of temperature dependent foraging behavior, digestive physiology, and temperature dependent metabolic expenditure. In endotherms, mass absorbed would be independent of temperature from the perspective of digestive physiology, if core temperature remains constant. However, temperature dependent foraging behavior at temperature extremes (dashed line) reduces food intake at temperature extremes, thereby creating an elliptically shaped region of discretionary mass whose value is temperature dependent. The optimum temperature for maximum discretionary mass decreases with increasing body size (see Fig. 13 below).

body temperatures that endotherms usually maintain. This is in contrast to the temperature dependent digestion of ectotherms (Waldschmidt *et al.*, 1987).

However, the temperature dependent foraging behavior and appetite levels of endotherms are frequently ignored, although they have been considered with respect to domestic animals (Kleiber, 1975). Recent seed tray experiments under natural foraging conditions show that desert rodents are extremely sensitive to substrate temperatures that affect willingness to forage (Mitchell *et al.*, ms), and similar results have been reported for free ranging raccoons (Berris, 1998). Predation risk and competition also influence foraging costs. Birds and mammals may compete for the same resource (Brown *et al.*, 1997). Predation risk and competition can be expressed in terms of energetic cost (Brown *et al.*, 1994).

Thus, the difference between temperature dependent foraging (mass and chemical energy intake) and temperature dependent metabolic costs (mass and chemical energy expenditure) yields temperature dependent discretionary mass and energy intake. Discretionary mass and energy intake is the oval area in Figure 5 bordered by intake and expenditure rates. Climate and type of food available are important constraints on fitness that can now be calculated from basic principles. As we shall soon see, body size and diet are additional important constraints on fitness in different climates.

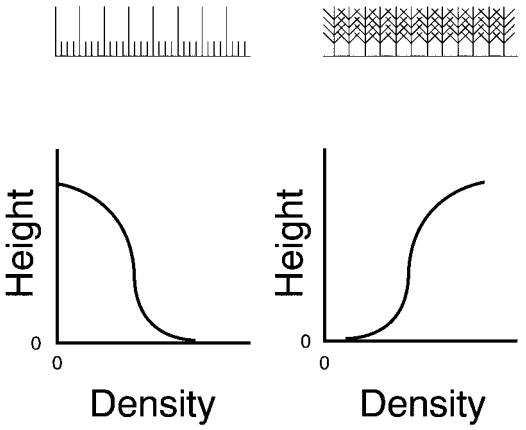

FIG. 6. A comparison of density profiles as a function of distance from the skin for fur (A) and plumage (B).

Porous insulation

Fur vs. feathers. Figure 6 shows schematically the difference between fur and plumage density as a function of distance above the skin. The densities of hair elements are greatest near the skin. The density of feather elements, in contrast, is lowest near the skin and greatest at the feather–air interface. The consequence of this difference in density profiles is that air can penetrate at least the outer parts of fur more easily. Feathers, however, seal off the plumage–air interface, creating a conduction–radiation environment that is easier to analyze.

This is true, irrespective of whether the fur or plumage elements are normal to the skin or at an angle relative to the skin. Changing angle relative to the skin modifies density profiles for either type of porous insulation, but does not change the general shape of the density profile with depth. In reality, parts of the skin of birds do have plumaceous elements near the skin. Individual plumages will vary between taxa and between different locations on the body. The density will also vary with degree of elevation of contour feathers, degree of density at the same level of the rachis/vane junction, and the presence and density of down feathers. However, vertical serial sections of crow feathers embedded in plastic under vacuum have shown that the greatest density of elements is at the plumage–air interface (Porter, unpublished data).

Fortunately, in low wind environments, changes in individual element density with height do not have a significant impact on porous insulation heat loss, unless the fibrous elements are either very sparse or extremely dense across a wide range of body sizes (Fig. 25 in Porter *et al.*, 1994). At very low individual element density, the porous insulation becomes very open, allowing substantial convective and radiant heat transfer from the skin. In contrast, at very high individual element density, the effective thermal conductivity of the porous insulation approaches that of keratin, rather than air. This amounts to an increase in thermal conductivity by a factor of about eight, thus increasing heat loss. Sensitivity of heat loss due to density changes with depth in fur in a conduction-radiation heat exchange is very small (Kowalski, 1978; McClure and Porter, 1983). Kowalski used a measured density of fur as a function of depth for cow fur, which is described by a hyperbolic tangent function (Fig. 6).

If fur density has an optical thickness (Porter *et al.*, 1994) less than 0.001, the fur is so sparse that it is assumed to be transparent to infrared radiation, and conduction heat transfer along the fibers is negligible. Under these conditions, the model assumes the functional equivalent of bare skin. For example, a user of the model can explore the consequences of changing insulation or removing insulation merely by altering the input data file, the depth and density of fur or plumage. If it is set to zero, or very low density, the program automatically checks to be sure that a porous model is appropriate and changes to a bare skin model, if necessary.

Finite elements and flow through the fur. Moderate and high wind environments can force penetration of air through fur. Thus, it was important to develop a basic principles model that would permit calculation of velocity and temperature profiles in a porous medium with nonlinear coordinates on a round body. Integration of the profiles allows for calculations of heat energy and mass transfer from basic principles, a task first accomplished only recently (Stewart *et*

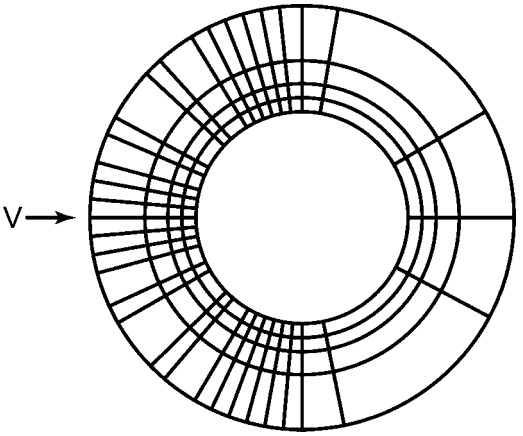

FIG. 7. A finite element model in cylindrical coordinates. The grid lines define curvilinear cells for simultaneous solutions of equations used in calculating mass and energy transport in the fur.

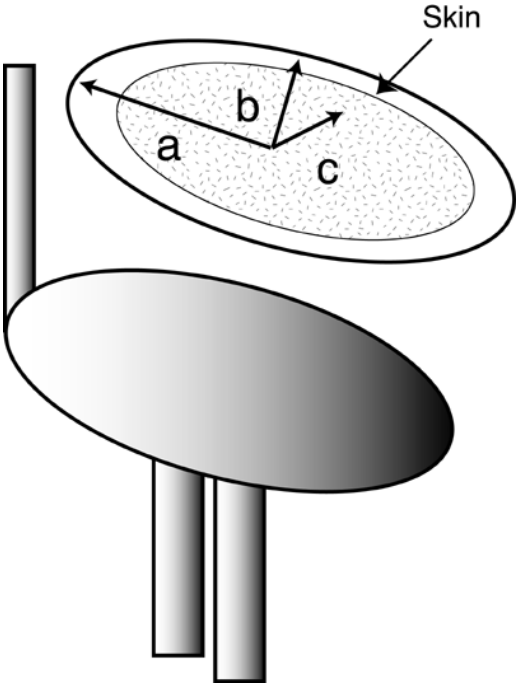

FIG. 8. Diagram of the geometries used to model a large standing bird (cylinders and ellipsoid) compared to a sitting bird (ellipsoid).

al., 1993; Budaraju *et al.*, 1994, 1997). We will briefly review the basic features of this sophisticated model.

Figure 7 shows the finite element model in cylindrical (radial and angular) coordinates from an end view. These curvilinear boxes are used to compute the mass and heat flows in the radial and angular directions relative to the skin and to the direction of incoming air for variable densities of keratin elements projecting from the skin of an endotherm. This concept is also appropriate for birds, under conditions where air penetrates the feathers. Examples include resting birds with fluffed feathers or flightless birds like kiwis, whose plumage strongly resembles mammalian fur. In principle, this model would also be useful for the pulsing (changing angular orientation relative to the skin) feather conditions of active bird flight.

Appendages. Figure 8 shows an appendage model for birds developed for three large ratites, the rhea, *Rhea americana,* the cassowary, *Casuarius casuarius,* and the ostrich, *Struthio camelus.* These appendages are largely bare and constitute a significant percentage of the surface area of the standing bird. Appendage dimensions were measured relative to torso dimensions using photographs of the birds of known height and weight from the side, and the front. We measured only the exposed areas of appendages. The portions of the legs covered by torso feathers were assumed to be part of the volume of the torso for heat transfer calculations.

The same cross-section model shown in Figure 2, but without porous insulation and respiratory water loss, was used to calculate heat loss in the radial dimension from these appendages. Heat loss from the bottom of the appendages in contact with the ground was assumed to be negligible. Total calculated heat loss was the sum computed from the torso plus the heat losses from the appendages.

The regression equations that were fitted to the appendage dimensions, areas, and volumes are listed in the Appendix. The appendage dimensions were computed from regressions based on body weight. Appendage volumes were then computed, added and the total subtracted from the total volume of the bird based upon its weight. The difference was the torso volume. The torso length, width, and height were calculated from the dimension ratios of the feathered

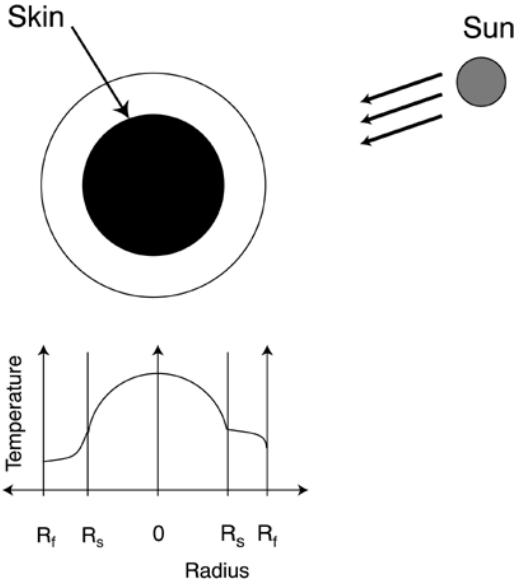

FIG. 9. Profiles of body temperature and insulation temperature. The left side, which is shaded, has a logarithmic profile in the porous insulation. The right side, which is exposed to sunlight, absorbs solar radiation in the fur and has a parabolic temperature profile, indicating heat absorption within the layer as well as heat transport within the layer.

torso. The calculated torso dimensions then were used to compute the effective torso skin area and plumage depths. Plumage depths agreed well with the few data available.

RESULTS

Modeling an individual

Internal body temperature profiles. Figure 9 demonstrates the temperature profile from core to skin to the insulation–air interface. The temperature profiles in the porous insulation (left side) represent no absorbed solar radiation *vs.* (right side) absorbed solar radiation. When sunlight is absorbed by a porous insulation, it will act as a distributed heat source in the medium ($R_s - R_f$). The color of the insulation and its transparency affect the depth over which the radiation is absorbed. The temperature profile from center to skin ($0 - R_s$) is parabolic in a slab, cylinder, sphere or ellipsoid with uniform heat generation per unit volume (Porter *et al.,* 1994: Appendix, equations 1–3). The temperature difference from core to skin is equal to the heat generation per unit volume multiplied by the radius squared divided by the product of a geometry constant and the thermal conductivity. The value of the geometry constant may be 2, 4, or 6, depending on whether the geometry is a slab/ellipsoid, a cylinder, or a sphere (Bird *et al.*, 1960; Porter *et al.*, 1994).

The calculation of distributed respiratory water loss had to take this parabolic temperature profile into account. The average temperature for a nonlinear profile can be calculated easily using an integration procedure (Bird *et al.*, 1960, p. 270). The volume average temperature was used as the average lung temperature for the purpose of calculating saturation vapor pressure. The amount of water lost in respiration was equal to the water added internally to saturate the air in the lungs at average temperature less the water recovered at saturation at the exit temperature at surface 2 in Figure 4.

The insulation. The flow of air through fur or plumage is influenced by the diameter and density of the fibrous elements the air encounters as well as the pressure generated in the flow field around the animal. We illustrate the combined effect of these variables on flow through fur in a red deer (*Cervus elaphus elaphus*) in Figure 10a, b, and c modified from Budaraju *et al.* (1997). Red deer fur is well characterized (Steudel *et al.,* 1994).

Flow at very low wind. Figure 10a shows calculated flow through the fur of red deer at 0.01 m/sec using the finite element model (Budaraju *et al.,* 1997). The streamlines shown are trajectories of airflow through the fur layer. Free convection is the dominant airflow pattern. Nearly still air in the vicinity of the animal enters at the bottom (ventral surface), flows along the sides of the animal and exits at the top (dorsal surface). The velocity is greatest near the skin along the sides of the animal, and least near the ventral and dorsal surfaces.

Flow at 0.5 and 3 m/sec. Figure 10b and c show calculated flow through the fur of red deer in a 0.5 and 3 m/sec wind using the finite element model (Budaraju *et al.*, 1997). Now the wind is assumed to be

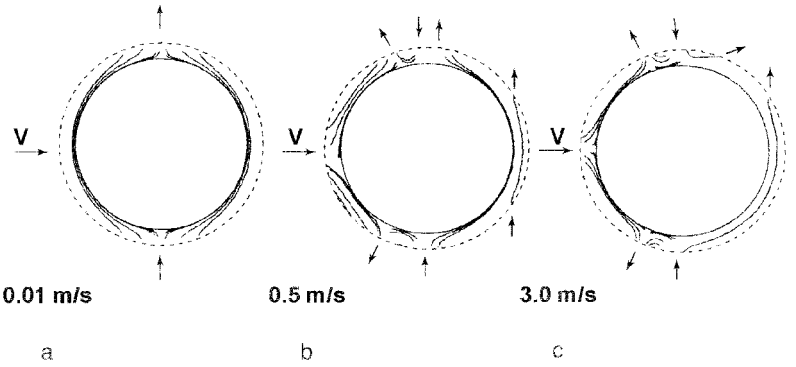

FIG. 10. Streamlines showing simulated air flow through red deer (elk) fur at 0.01 m/s external wind speed (a). Streamlines showing simulated air flow through red deer fur at 0.5 and 3.0 m/s wind speed (b) and (c).

blowing horizontally from left to right. The long axis of the body is assumed to be normal to the direction of wind flow. The streamlines diverge on the windward side, enter the fur, and then move toward the dorsal and ventral parts of the animal. Air recirculates near the top and bottom because of pressure differences that are a consequence of the geometry and the properties of air. A recirculating eddy then enters the fur, moving toward the leeward side of the animal and finally exits the fur.

We might expect similar types of air movement if birds fluffed their feathers at rest in a moderately strong wind, where air could enter the plumage from the windward side. However, birds typically only fluff their feathers in very low wind environments. Figure 10a suggests that extending the insulation further laterally and normal to the flow might slow free convection around the body.

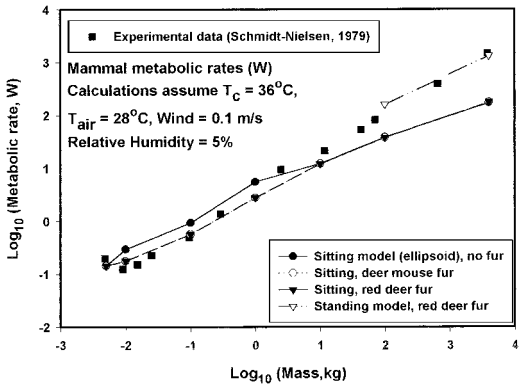

FIG. 11. A comparison of measured *vs.* calculated metabolic heat production for animals ranging in size from mice to elephants. The diamonds represent the empirical data collected at a body temperature of 36°C and an air temperature of 28°C. An ellipsoid model is assumed for an animal lying down. At this low (metabolic chamber) wind speed and humidity the presence or absence of fur makes little difference in the metabolic cost.

Scaling across mammal body sizes

Mouse to elephant metabolic rate. Skin temperature is a consequence of the solution of heat flux equation (the correct guess of heat generation to maintain core temperature) from the core to the skin. It is simultaneously the basis for heat exchange from the skin through the porous insulation to the environment. The total heat generation must satisfy the coupled body and insulation equations whose boundary conditions are core temperature and environmental conditions.

Figure 11 shows these heat generation calculations assuming an ellipsoid geometry for animals ranging in size from mice to elephants. The line with filled circles assumes a bare skin. Alternatively, if we put deer mouse (*Peromyscus maniculatus*) fur on all body sizes instead, we get the line with open circles on it. The free-floating diamonds represent the empirical data.

An appendage model was also developed for mammals using the same principles as just described for birds. However, the torso, head, and neck were assumed to be cylindrical in shape with an elliptical cross section. The ratio of the elliptical cross-section

based on photographic measurements of elephants and cattle was 1.27 for the ratio of height to width of the torso. The appendage model was not used for animals smaller than 100 kg.

It is particularly interesting to note that for the *standing* mammal model using no fur *vs.* fur of red deer (a form of elk), there is no observable difference in metabolic rate from 100 kg to 3,833 kg. This is reasonable, since the low wind speed used here would probably not disrupt the substantial boundary layer of these large mammals. Fur would be of little help at this low wind speed in an environment where the air and radiant temperatures are assumed to be the same.

It is important to note that the experimental data in the literature used to test this model were all collected in a metabolic chamber at an air and radiant temperature of 28°C and a core temperature of 36°C. Benedict measured the core temperature of all of his animals in his classic publication (Benedict, 1938). A sensitivity analysis of the conduction–radiation fur model shows that core, air and radiant temperatures are the most sensitive of all variables affecting heat loss from an animal with porous insulation (McClure and Porter, 1983).

Figure 12 illustrates the impact of changing air temperature on the mouse to elephant curve. The frame of reference is the experimental data shown as free-floating diamonds. A simulation for 28°C is the dashed line with open circles. Metabolic rates at a lower temperature of −25°C and an upper temperature of 40°C are also calculated. The increase in metabolism at small body size for 40°C air temperature is part of a consequence of the thermoregulatory model used in these calculations. It is an emergent property of the model.

It is also important to realize that the postures of Benedict's animals were largely unknown. In fact, posture is rarely monitored in metabolic rate measurements. Metabolic costs can vary considerably due to simple changes in posture (Porter *et al.,* 1994). Ellipsoid geometry is the best intermediate approximation for estimating metabolic costs in mammals (Porter *et al.,* 1994).

The term ''thermal conductance'' is an

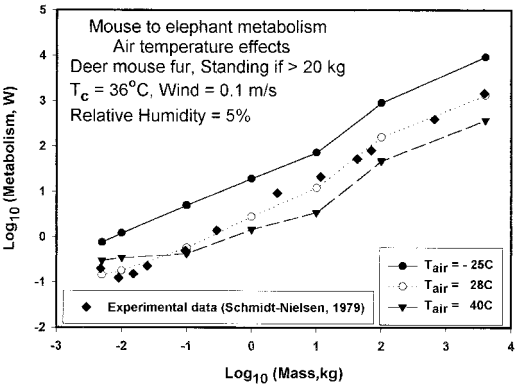

FIG. 12. Calculated metabolic rates *vs.* body mass and environmental temperature for animals ranging in size from mice to elephants. The 28°C line represents the Benedict's experimental environment used to collect the empirical data. The low and high temperature calculations indicate that metabolic scaling with body size is dependent on environmental temperature. The 40°C curve approaches the 0°C curve at small body masses because heat stress is forcing the metabolic rate to high levels. No empirical regressions are used in these calculations other than appendage morphology as a function of body mass.

amalgam of all the variables associated with specific morphological, physiological and climate variables. Those state variables have been explicitly defined in an appendix (Porter *et al.,* 1994), where the detailed equations for the model reside. The metabolic heat lost by an animal is a consequence of (1) body morphology and insulation properties, (2) core temperature and thermal conductivity of body tissues, and (3) environmental conditions, such as air temperature, sky radiant temperature, ground radiant temperature, and wind speed. *Solar radiation and relative humidity* were not explicitly included in the earlier endotherm model (Porter *et al.,* 1994), but they *are added in the present model.*

Figure 12 demonstrates the limitations of the regression assumptions in the standard mouse to elephant metabolism regression line when applied to natural environments. The slope and intercept of the mouse to elephant curve changes with air/radiant temperature and body size.

Mouse to elephant discretionary energy uptake. Figure 13a and b show explicitly the calculated discretionary energy uptake for mammals of different sizes represented

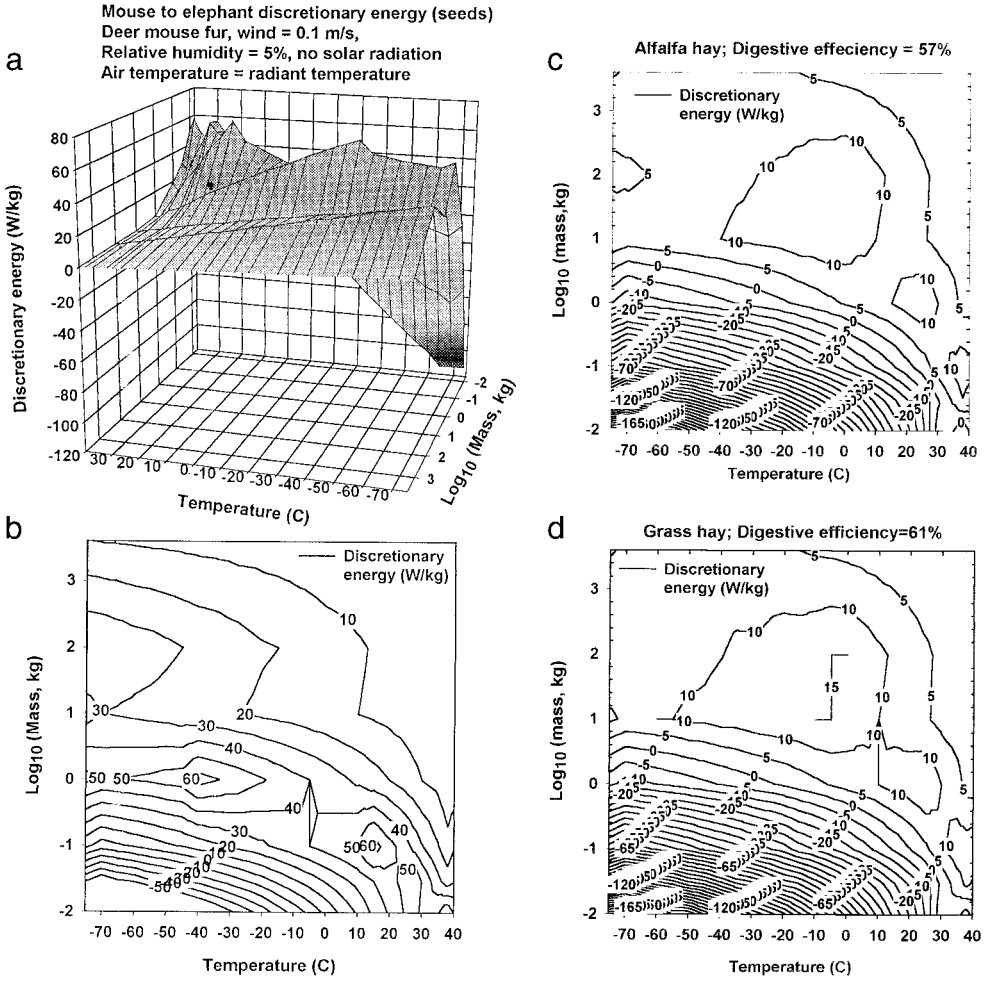

FIG. 13. A topographic view of the log of discretionary energy uptake (J/day) as a function of log of body mass and environmental temperature. Air and radiant temperatures are assumed equal. There is a ''ridge'' of maximum discretionary energy (fitness measure) that is irregular in elevation as it curves upward and to the left in Figure 13b from its starting point at about 28°C. where the body size is 0.01 kg. As body size *increases,* the *optimal environmental temperature* that maximizes discretionary energy for body size *decreases.* The discretionary energy maximum traces a jagged ridge with peaks and valleys going to lower and lower temperatures. This result occurs because of differences in the temperature at the lowest metabolic rate for animals of different sizes and the maximum limit on gut mass flow per day at each body size. The temperature associated with maximum distance between those two curves changes with body size.

Figure 13a and b were calculated assuming a diet of seeds for all body sizes. The proportions of carbohydrate, fats and protein in the dry matter are similar to those of alfalfa hay and grass hay forage (see Appendix). When the diet is assumed to be alfalfa hay (reference number 100056; U.S.–Canadian nutrient composition tables, 1994) with the same digestive efficiency of 57% as for seeds, Figure 13c shows a similar optimal body size landscape, but the ''ridge'' is shifted to larger body size for the same temperature. The magnitude of the ''peaks'' is much reduced. The landscape is also much flatter. The body size where the animal is in negative mass balance is much larger for the same temperature.

Figure 13d shows the landscape for an assumed diet of grass hay (reference number 102250; U.S.–Canadian nutrient composition tables, 1994) for mice to elephants. The digestive efficiency is 61%, to reflect the overall digestive ability of ruminants. This makes for slightly higher peaks but the same general landscape. The change in digestive efficiency more than compensates for the change in quality of diet. Thus, when examining all three contour plots, *the higher the quality of diet, the smaller the optimal body size at any given temperature.*

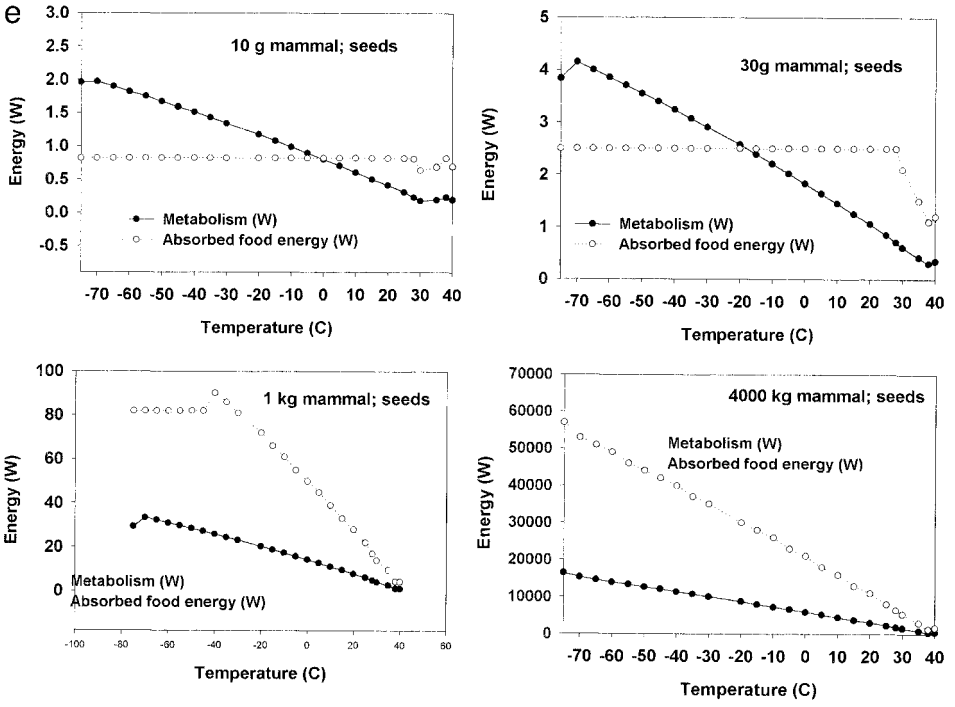

Figure 13e compares four different sizes of mammals all assumed to be consuming seeds as their diet. The 10 g mammal has a net throughput capacity that matches metabolic cost slightly below 0°C. Temperatures lower than this we calculated will cause the animal to be in negative mass balance without an insulating nest or change in posture (Porter *et al.*, 1994). A 30 g mammal has the same intersection at approximately −18°C. A one kilogram mammal has a body size large enough to assure adequate gut mass flow until approximately −40°C, assuming deer mouse fur and appendages that are extended. If a 4,000 kg mammal were able to process seeds of the same nutritional properties as the smaller mammals, it would have sufficient gut throughput to allow it to have no mass flow constraints, even with only deer mouse fur at this very low wind speed of 0.1 m/s.

qualitatively in Figure 5. Selection for maximum discretionary energy uptake represents selection for growth and reproduction potential, key elements of fitness. The three dimensional and the contour map of body size and temperature effects on discretionary energy uptake assume no food limitation. The animals are simply allowed to fill their gut, digest and absorb the food. At temperatures where sweating must be initiated to cool the animal, it is assumed that animals no longer forage. These figures are an upper estimate of discretionary mass intake as a function of body size. Air temperature is assumed to be the same as the radiant temperature of the sky and ground. Thus, this set of calculations represents metabolic chamber environments. The effects of changing wind, sunlight and humidity are not included in these figures.

A very interesting feature of the three dimensional and contour surfaces is the suggestion of discontinuous optimal body sizes in nature, where temperature varies in time and space. There is a ''ridge'' of maximum discretionary energy (fitness) that is irregular in elevation as it curves upward and to the left in Figure 13b from its starting point at about 28°C where the body size is 0.01 kg body size. As body size *increases,* the *optimal environmental temperature* that maximizes discretionary energy for body size *decreases.* The discretionary energy maximum traces a jagged ridge with peaks and valleys going to lower and lower temperatures. This result occurs because of differences in the temperature at the lowest metabolic rate for animals of different sizes and the maximum limit on gut mass flow per day at each body size. The temperature

associated with maximum distance between those two curves changes with body size. Thus, the greater payoff in discretionary energy (fitness) at some temperature/body size combinations relative to others of lower value at nearby temperatures suggests there should be a selection for the size that has the highest value in the neighborhood of a small temperature range. This would create one or more ''gaps'' in the distribution of animal sizes in nature. The largest gap shown here is between −5 and 0°C and a body size of approximately 100 kg.

Diet effects on optimal body size. Figure 13a and b were calculated assuming a diet of seeds for all body sizes. The proportions of carbohydrate, fats and protein in the dry matter are similar to those of alfalfa hay and grass hay forage (see Appendix). However, the water content is very different. When the diet is assumed to be alfalfa hay (reference number 100056; U.S.–Canadian nutrient composition tables, 1994) with the same digestive efficiency of 57% as for seeds, Figure 13c shows a similar optimal body size landscape, but the ''ridge'' is shifted to larger body size for the same temperature. The magnitude of the ''peaks'' is much reduced. The landscape is also much flatter. The body size where the animal is in negative mass balance is much larger for the same temperature.

Figure 13d shows the landscape for an assumed diet of grass hay (reference number 102250; U.S.–Canadian nutrient composition tables, 1994) for all animals ranging in size from mice to elephants. The digestive efficiency is 61%, to reflect the overall digestive ability of ruminants. This makes for slightly higher peaks but the same general landscape. The change in digestive efficiency more than compensates for the change in quality of diet. Thus, when examining all three contour plots, *the higher the quality of diet, the smaller the optimal body size at any given temperature.*

Figure 13e compares four different sizes of mammals all assumed to be consuming seeds as their diet. The ten gram mammal has a net throughput capacity that matches metabolic cost slightly below 0°C. Temperatures lower than this we calculated will cause the animal to be in negative mass balance without an insulating nest or change in posture (Porter *et al.,* 1994). A 30 g mammal has the same intersection at approximately −18°C. A1 kg mammal has a body size large enough to assure adequate gut mass flow until approximately −40°C, assuming deer mouse fur and appendages that are extended. If a 4,000 kg mammal were able to process seeds of the same nutritional properties as the smaller mammals, it would have sufficient gut throughput to allow it to have no mass flow constraints, even with only deer mouse fur at this very low wind speed of 0.1 m/sec. A quick examination of the maximum distance between the two curves of the four sizes of animals shows different temperature optima where maximum discretionary energy is available assuming unlimited seeds. As we saw from Figure 13c and d, a change in diet from seeds to green forage shifts the optimum body size at any given temperature to higher values. These results ignore coprophagy and other subtle, but significant modifications of digestive systems. Nonetheless, it provides some useful guidelines for identifying future modifications of the gut model and provides some understanding of multiple constraints on optimal body size of animals.

Bergmann's Rule. These results are reminiscent of Bergmann's rule, an empirical observation that as climates get colder, animal sizes tend to get larger. Body size increases with decreasing temperature provide the greatest advantage at small size (Steudel *et al.,* 1994). At larger body sizes, changes in fur insulation confer a greater advantage Steudel *et al.,* 1994). Experimental data from different types of fur on a flat plate (Scholander *et al.,* 1950) suggested this, but animals of larger size also have thicker boundary layers. A thicker boundary layer reduces convective heat loss and simultaneously enhances radiation temperature effects (Porter and Gates, 1969). Larger animals are taller, which means exposure to greater wind speeds higher above the ground. Higher wind speed reduces boundary layer thickness and may engender greater wind penetration of the fur. A first principles fur model can separate boundary layer effects due to size and wind from fur

properties effects and provide better estimates of combined effects.

Assessment of consequences of Bergmann's rule have pointed out that larger animals have the advantage of longer fasting ability under conditions of climate or food availability stress (Morrison, 1960). However, smaller animals have the advantage of lowering body temperature and seeking much more favorable microclimates, especially underground habits in severe cold. Careful transient modeling analyses of these two strategies in the animals' microclimates would yield a testable hypothesis of the relative benefits of these different solutions to the same problem of dealing with cold.

Of course, survival in extreme temperature events is also important in affecting community structure. However, extreme temperature survival may be overrated in terms of its effects on community structure, at least for mammals. Temperature dependent behavior and selection of microhabitats by both small and large animals can greatly reduce cold or heat stress. For example, moving under or into trees and modifying the solar and infrared radiation and wind protection they provide can change equivalent local microenvironment temperatures by 20°C or more. Underground burrows or tunneling beneath the snow can provide habitats that typically do not drop below 0°C in winter when an animal is present, due to local heat from metabolism. Photoperiod-induced temperature dependent physiology, such as hibernation or estivation is another way that mammals can persist in habitats during periods of extreme heat or cold stress and thereby maintain community structure. Birds typically opt to migrate from extremely cold habitats in winter that they occupy in the summer. By exercising temperature dependent behavioral selection of microclimates through migration, the scale of their selection movements is simply larger due to the short time and lower costs of long distance bird transport.

Scaling across bird body size

Hummingbird to ostrich metabolic rate—Appendage effect. Figure 14 shows the impact of appendages on heat loss in large birds by comparing data on bird metabolism with calculations of bird metabolism using two different models. The filled circles represent bird metabolism *vs.* body size in the absence of sunlight (Schmidt-Nielsen, 1979). The sitting bird model calculations use an ellipsoid approximation for a bird with legs and head tucked into the feathers. The standing bird model represents the torso as an ellipsoid, and the appendages as cylinders with diameters averaged over the appendage length. The solid line marked with solid triangles is the sitting bird model. We assumed an air temperature and radiant temperature of 30°C. The dashed line with open triangles represents the standing bird model calculations only for the ratite birds; rheas, cassowaries and ostriches. All smaller birds are assumed to be sitting. We assume that the birds are maintaining a core temperature of 39°C at the center of the torso and at the centers of the appendages.

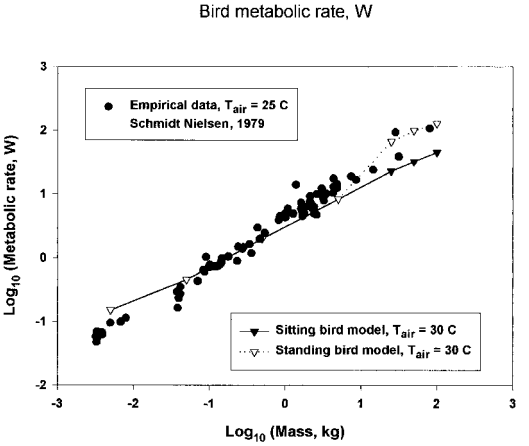

FIG. 14. The calculated effect of posture on metabolic rate in birds (solid *vs.* dashed line). The birds range in size from hummingbirds to ostriches. Open triangles attached to lines represent the calculated values for large standing birds. The calculated values for sitting birds are represented by the closed triangles on the solid lines. The empirical data (summarized in Schmidt-Nielsen, 1979) are free floating filled circles. Environmental temperatures used to obtain these empirical data were approximately 25–30°C.

Hummingbird to ostrich metabolic rates—Air temperature effect. Figure 15 demonstrates the effect of air temperature on metabolic rates as a function of bird

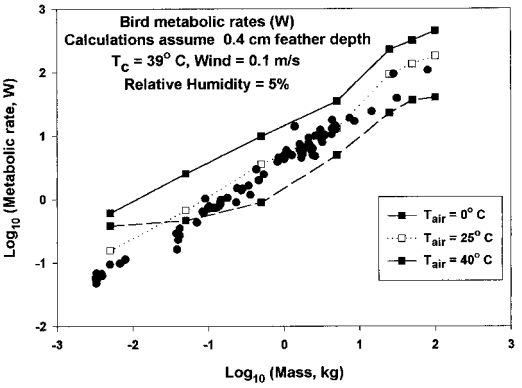

FIG. 15. The calculated effect of temperature differences on metabolic rate for birds ranging in size from hummingbirds to ostriches. The 40°C curve approaches the 0°C. curve at small body masses because heat stress is forcing the metabolic rate to high levels. No empirical regressions are used in these calculations other than appendage morphology as a function of body mass.

body size. As in Figure 14, we assumed that air and radiant temperatures are the same and there is no significant sunlight. The calculations at 0°, 25°, and 40°C assume that large birds (mass 10 kg or greater) are standing up. At 40°C small birds are predicted to have high metabolic rates, because they would be in heat stress.

Global communities-climatic constraints

Figure 16 shows temporal and spatial variation in optimal body size based on discretionary mass/energy for mammals for the months of January and July on a global scale. In January (winter) in the Northern Hemisphere, the optimal sizes are larger as one moves north. Large topographic features, such as the Rocky Mountains, are also predicted to have larger animals with their optima. In the Southern Hemisphere, where it is summer, topographic features do not stand out as strongly.

In July (winter) in the Southern Hemisphere there is somewhat of a ''mirror image'' effect on optimal body size. However, different topographic and latitudinal features create somewhat different patterns. In general, though, the model suggests that larger animals have the advantage. In the Northern Hemisphere at the same time smaller animals should have the advantage. Large topographic features like the Tibetan plateau with its cool weather in summer still show up fairly clearly as affecting optimal body size. For clarity, variation in vegetation type and food quality were not included in these graphs.

The criteria for optimization were maximum discretionary energy uptake for a given temperature at all possible body sizes. This figure was generated from the endotherm model driven by global weather data at half-degree intervals in latitude and longitude.

The map of optimal body size is different at different seasons of the year. This suggests that climate places important constraints on what functional types can coexist in a locality. Because the environment is constantly changing, it creates a constantly changing optimal body size in any locality. Changing environments create the opportunity for multiple functional types to coexist in the same area.

What is unknown at present is over what time intervals does natural selection integrate time and environmental conditions to ''choose'' body size? Figure 16 represents the beginnings of the effort to understand climatic constraints on community structure from basic principles. The vegetation on the landscape is certainly a very important variable that will modify the current version of the model. The spatial and temporal distribution of available food places important additional constraints on optimal body size. These constraints include encounter probabilities, handling time, food energy value and metabolic cost to get to the food. Three of these variables are related to body size and the ''packaging'' and ''distribution'' of

→

FIG. 16. Calculated optimal mammal body size that maximizes discretionary energy uptake as a function of global temperatures in January and in July. No food limitation or variation in food type is assumed. These results suggest that climate variations in time and space place important constraints on the functional types of animals that can coexist as communities.

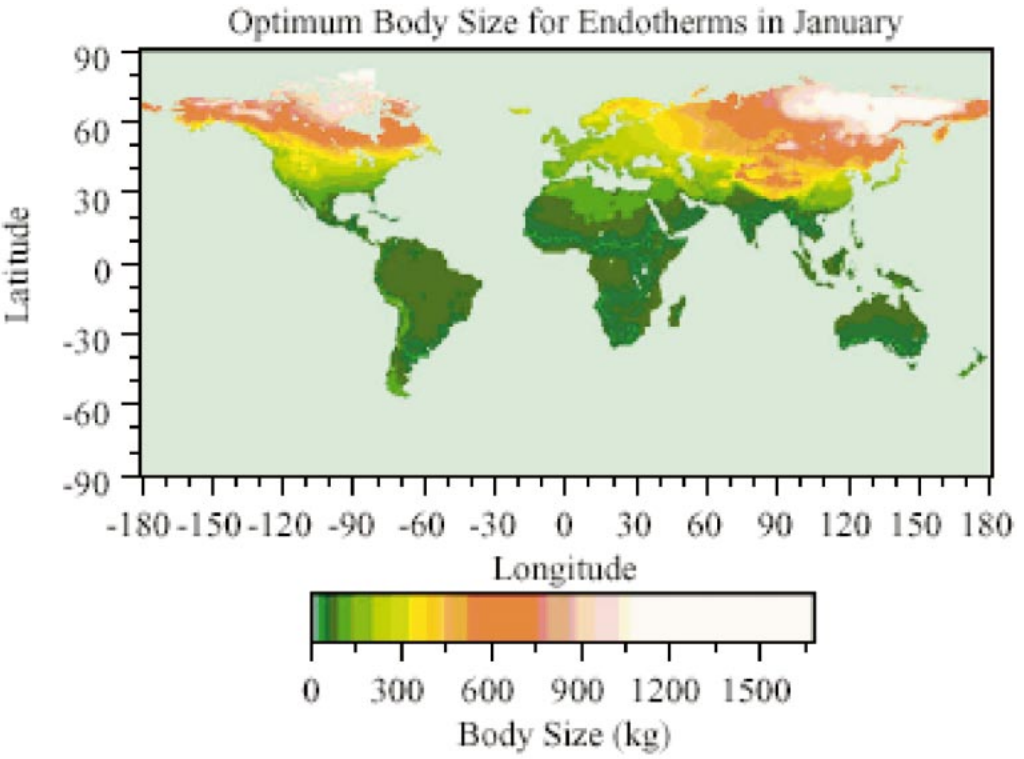

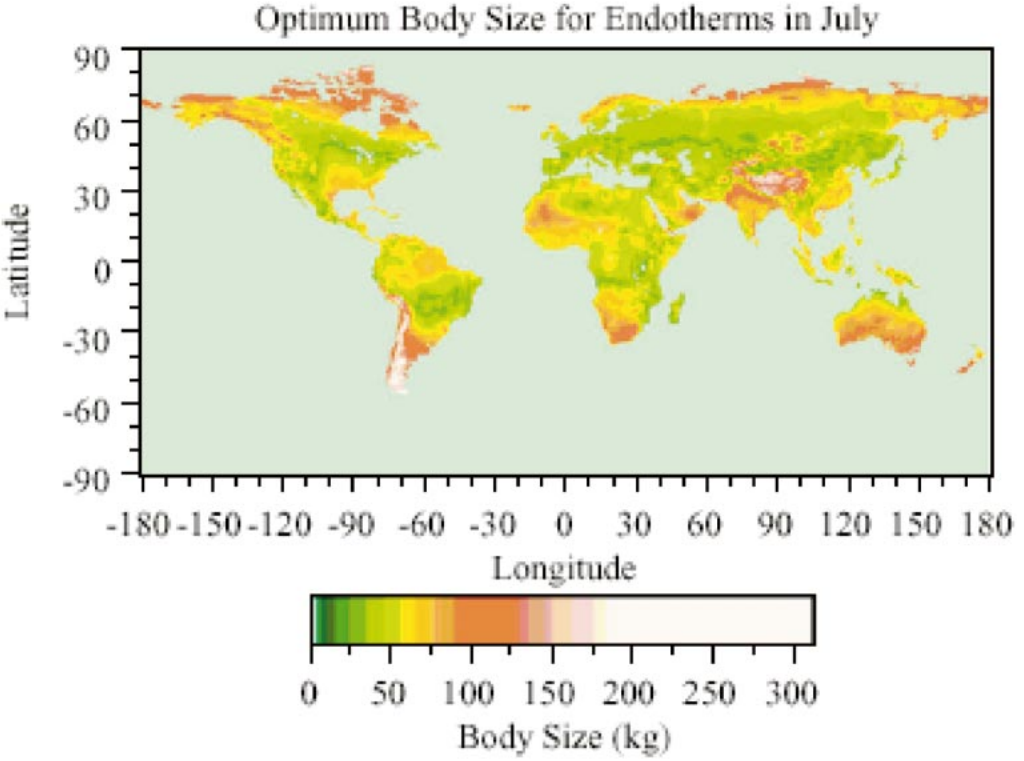

FIG. 17. The rare and endangered Orange-bellied Parrot of Australia and Tasmania.

food on the landscape. It is clear that this construct can also be applied to species of birds to study migratory patterns and other aspects of bird ecology.

It is important to note, as one reviewer did, that ''evolution may select less for optima under average daily climate cycles and more for adaptations that increase survivorship during winnowing events. At any given time a population may consist of individuals with below or above optimal body sizes, should recent history include high mortality linked to extreme climate, with availability, or predation.'' These important considerations have not been added to these models yet.

Conservation application: The Orange-bellied Parrot, Neophema chrysogaster

The Orange-bellied Parrot (Fig. 17) has only approximately 200 individuals still alive. It breeds in Tasmania. After the young have fledged the parents fly north for the winter to the southern coast of Australia. The young follow shortly thereafter (Hutchins and Lovell, 1982; Loyn *et al.*, 1986). There is nothing known about their metabolic rates and little about their physiology, although it is now known that core temperature is maintained at about 41.1°C (P. Menkhorst, personal communication). There are important energetic questions that may pertain to the species' survival. It appears that survival during the winter season is more important than their reproductive success in summer (Drechsler *et al.*, 1998). Food supplies in nature, particularly Sea Rocket, appeared to have dwindled, but they have shifted somewhat to other plants. Numbers of individuals in the last few years seem to have stabilized (P. Menkhorst, personal communication). The causes of the Orange-bellied Parrot's decline remain an enigma. If there were reliable estimates of metabolic cost, estimates of necessary foraging time and amount of food required to sustain it in its seasonal habitats could be made. This could lead to quantitative estimates of the amount of habitat needed to assure its survival, especially in what appear to be its critical northern wintering habitat.

Ontogeny of metabolic costs. We are aware of only two papers in the literature on parrot metabolism (Bucher, 1983; Bucher and Morgan, 1989). Bucher's metabolic chamber data can be used to test the bird model for metabolic chamber conditions. Figure 18 shows that the model can closely approximate experimental data on an African parrot, *Agapornis roseicollis,* the peach-faced lovebird, of similar weight and dimensions as the Orange-bellied Parrot. We can calculate parrot metabolism across the experimental temperature range that the bird experienced. This allows us to have more confidence when extending the model to field conditions to estimate its energy use requirements in its native habitat. We calculated metabolic rate up to air/radiant temperatures of 40°C, even though experimental measurements only go to 35°C.

Calculations for low air temperatures agree best when a spherical posture is assumed, a lower 41.1°C core temperature is used as was measured (Bucher, 1983; Bucher and Morgan, 1989), and the feathers are somewhat fluffed (0.7 cm). At higher air temperatures, an ellipsoid approximation with slightly higher core temperature (41.4°C) and normal plumage depth (0.4

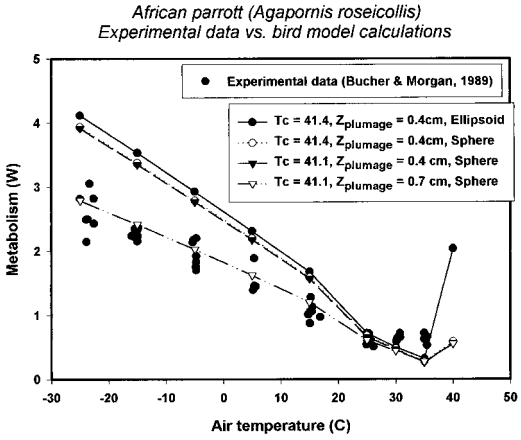

FIG. 18. Comparison of bird model calculations vs. measured metabolic rates for a 48 g African parrot, *Agapornis roseicollis,* the peach-faced lovebird. Experimental data covered the temperature range from −25°C. through 35°C (Bucher and Morgan, 1989). The model calculations explore changes in posture (ellipsoid *vs.* sphere). Observed range of variation in core temperature was 41.1°–41.9°C (Bucher and Morgan, 1989). Feather lengths of normal plumage we measured from U.W. Zoology Museum specimens ranged from 1.0–1.5 cm. Depth of plumage was typically 0.4 cm. We assumed fluffing of feathers would change feather depth from 0.4 to 0.7. Calculated results agree with data best if the birds in the cold are placing their head under their wing and fluffing their feathers to 0.7 cm depth. At higher temperatures calculations agree with data best when postures approximate an ellipsoid, there is a slightly higher core temperature, and the feathers are not fluffed. An ellipsoid model calculation assuming a core temperature of 41.9°C. (measured by Bucher and Morgan [1989] at 30° and 35°C.) was done too, but the results were nearly identical to the ellipsoid model with a core temperature of 41.4°C. and a plumage depth of 0.4 cm.

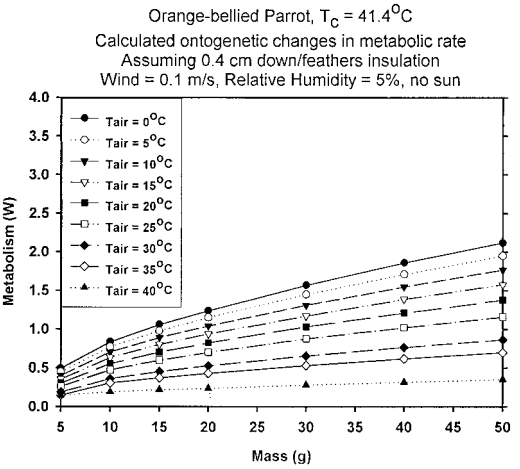

FIG. 19. Current estimates of metabolic rate through the ontogeny of the Orange-bellied Parrot with an observed core temperature of 41.1°C (P. Menkhorst, personal communication) for air/radiant temperatures ranging from 0°C. to 40°C.

cm) agree best with the experimental data. It would seem that plumage depth clearly has a greater impact than either postural change or core temperature change for a bird this size in a low wind speed environment lacking sunlight.

Figure 19 shows our current estimates for metabolic rate as a function of the ontogeny of the Orange-bellied Parrot. These metabolic chamber simulations use current estimates of insulation thickness of the down and feathers of the birds. The results indicate that temperatures lower than 5°C would be a challenge for hatchling birds. Temperatures below 20°C at weights of 20–40 g impose significant additional metabolic costs on young birds. This might be reflected in reduced potential for growth at these lower temperatures. Minor modifications in the gut model that include reasonable estimates of the range of foodstuffs ingested can be used to estimate growth and reproductive potential as the birds grow. That is the next step in our research on these birds.

DISCUSSION

Surrogates for size in modeling metabolism. Body weight is a surrogate for body radius. Posture is a surrogate for body geometry. Empirical metabolism data collected since the time of Benedict in the 1930s have related metabolic heat production to body mass. However, mass is only one of the variables that drive metabolic heat production. A key variable is the radius of the trunk of the animal, which is in turn a function of the posture. Most of the analyses of metabolic scaling in the literature that we know ignore this important aspect. Furthermore, the role of a variety of environmental variables and different types of porous insulation in modifying metabolic demand have not been predictable because of the lack of reliable quantitative models.

However, our new animal models and the microclimate model that links them to mac-

roclimate data have changed the outlook for understanding the quantitative relationships of these variables. Fortunately, there have been some careful experiments on endotherm heat loss in wind tunnels with solar radiation. They make it possible to test these models in much more realistic settings than metabolic chambers (Bakken, 1991; Bakken and Lee, 1992; Bakken *et al.*, 1991; Hayes and Gessaman, 1980, 1982; Rogowitz and Gessaman, 1990; Walsberg, 1988*a, b, c*; Walsberg and Wolf, 1995).

Climate/body size effects on biodiversity. Body size affects discretionary mass and energy intake. Growth and reproduction potential affects fitness. As Figures 11 through 15 demonstrate, body size has important impacts through geometric form and radial dimensions on energy expenditure and intake. The surrogate for these primary variables is body weight (mass). We have pointed out here how air and radiant temperature and posture can make important modifications in energy cost in different environments. These energy costs are not linear with body size. Heat transfer mechanisms are not all linear with body size and neither are temperature regulation responses. Scaling of the gut is not linear with body size, either (Calder, 1984). The combinations of these nonlinear functions result in calculations that suggest discontinuous optimal body size with temperature. This is consistent with empirical data (Brown *et al.*, 1993; Brown and Maurer, 1987; Brown and Nicoletto, 1991; Holling, 1992; Maurer *et al.*, 1992; Peterson *et al.*, 1998). However, there is an important reanalysis questioning these empirical results (Siemann and Brown, 1999). Our results of climate/body size/gut modeling suggest that whether or not animal sizes are clumped in nature may depend on the digestive efficiencies of foods consumed and the locations of those foods. High quality foods suggest greater clumping, low quality foods suggest very little in the way of body size clumping (Fig. 13a–d).

Body size effects on cost of foraging: temperature dependent foraging/activity time. Body size has multiple effects on cost of foraging. It affects heat and mass balance (Figs. 12, 13, 15, and 16). Body size affects cost of locomotion, which is constrained by the respiratory and mitochondrial systems of animals, as Taylor and his colleagues have so eloquently demonstrated (Mathieu *et al.*, 1981; Taylor *et al.*, 1982; Weibel *et al.*, 1991). Their studies interface very nicely with recent work on animal scaling (Enquist *et al.*, 1998; West *et al.*, 1997, 1999).

The work presented here explains that changes in boundary conditions, such as environmental constraints on heat and mass exchange, alter fluxes and therefore alter internal scaling requirements that must adapt to changing needs. Thus, we suggest that temperature dependent behavior may be an important response to environmental change that tends to keep the organism as close as possible to optimal function as dictated by its internal and external anatomy, thereby maximizing fitness.

Body size determines whether a species can be fossorial or not, which affects diurnal microclimates and heat and mass balances. Body size affects likelihood of predation, which can be cast as a cost of foraging (Brown *et al.*, 1994). Body size affects competition, which alters temperature-dependent activity time, which also affects cost of foraging.

Body size effects on total annual activity time. Body size effects on total annual activity time are mediated through heat and mass exchange with the environment. The onset of heat or cold stress appears to be an important constraint in limiting activity. That is, temperatures that force skin temperatures below 3°C or conditions where evaporative water loss must be elevated to protect organism integrity are bounds on activity time that impact animal fitness.

The boundary layer thickness in the air next to the animal surface constrains mass and heat transfer from an animal. Boundary layer thickness is a function of the friction between the animal surface and the air. The amount of friction depends on the dimension of the animal, fluid and animal speed relative to each other, and fluid properties of density, viscosity and thermal conductivity. On the one hand small animals have thin boundary layers and are more respon-

sive to convective environments than to radiant heat exchange (Porter and Gates, 1969). On the other hand, large animals have thicker boundary layers and are more sensitive to the diurnal changes in infrared radiation and solar radiation fluxes in the environment. For large animals, absorption of radiant energy is a much greater challenge, since cooling by convective heat transfer is diminished because of the thicker insulating boundary layer around the larger animal.

Body size affects competitive success, hence temperature-dependent behavior including habitat utilization, which impacts on total annual activity time.

Vegetation/body size effects on biodiversity. Vegetation modifies microclimate conditions available to animals in predictable ways. Animal body size determines where animals spend their time in the wind patterns near the ground. Figure 16 is based on empirical climate data. Those empirical data reflect how vegetation may modify local microclimates. Vegetation also affects animal energetics either by direct shading of the animals or by providing cool surfaces that radiate back to animals. Thus, by directly and indirectly affecting the animal heat fluxes, vegetation impacts optimal body size and constrains functional types that might coexist in a community.

The distribution and quality of food in space and time changes in an annual cycle. Animal food encounter probabilities, and food handling time are consequences of vegetation structure and type. The calculations used in Figure 16 do not yet incorporate various possible distributions of food of various types in the environment. Diverse food distributions have not yet been explored using our models. Food encounter probabilities and handling times, which are a key part of food intake, are only beginning to be explored. The different food types, sizes and spacing also place important constraints on the range of body sizes of animals, which can efficiently utilize them.

Body size, cost of locomotion, and home range size are also interconnected. Home range size must be a function of body size, cost of locomotion, and the foraging thermal and vegetative environment. The minimum time and cost to forage for a particular type, distribution and size of food should be calculable for a broad range of body sizes and environments.

Feathers and plumage. When we watch the development of feathers through the ontogeny of a bird, it is apparent that the down structure is very much like the extremely dense fur of some mammals. Both types of fibers emerge from single openings in the skin as multiple fibers and then ''fan out'' in three dimensions as multiple fibers as they grow. In so doing they extend the layer of still air above the skin (and in the insulation) substantially. The second stage of plumage development with the eruption of feathers that tend to seal off air flow even further from the skin is unique in its efficiency of cross linking elements to hold complex units together and seal out air flow. The only fur that seems even closely comparable is that of the snowshoe hare that has fur tips that are flattened like tiny shovels (Porter, unpublished data). These structures probably assist in minimizing air and snow penetration into the coat.

The restriction of feather tracts to portions of a bird's skin provide for flexibility in opening up skin areas to much more rapid heat transfer is also unique to birds. Some mammals like polar bears have inguinal regions that are highly vascularized and lightly furred. Polar bears sometimes apply them to the snow to dissipate heat, but mammals, unlike birds, have not evolved the ability to open large areas of nearly bare skin to dissipate or absorb heat.

CONCLUSIONS

1. Temporal and spatial variation in physical environments impose important constraints on functional types of animals that can coexist in biological communities. These constraints are further refined locally by food diversity representing different digestive qualities.

2. Morphology, physiology, and temperature-dependent activity in animals link individual energetics to population dynamics and community structure by specifying total

annual activity time and mass/energy available for growth and reproduction.

3. Porous insulation in birds at rest can be modeled with current state-of-the-art fur models. Resting birds have feather positions that tend to seal off convective transport. This creates a conduction–radiation heat transfer environment. This is simpler to calculate than an environment where three heat transfer mechanisms are all important.

4. Posture plays an important role in metabolic heat loss. This is true mainly because posture affects the radial dimension of the animal, which is a key variable in the equation governing an animal's total heat generation requirements. Posture is typically ignored in metabolic chamber metabolism studies. The model presented here allows the calculation of the upper and lower limits of metabolic expenditure for a wide variety of climatic conditions.

5. Animal geometry and posture, insulation properties, and environmental conditions influence ''thermal conductance.'' Thermal conductance is a term implying a passive transport of heat through a nonheat-generating medium. Thus, it is inappropriate for describing fluxes through flesh, where heat generation is occurring. It is also inappropriate in porous media that ''act alive'' by absorbing solar radiation in the insulation. Thermal conductance is affected by properties and boundary conditions that can have nonlinear effects on heat transport through the medium in question. It can be useful as a descriptive concept for heat source-free systems if all of the relevant boundary conditions and properties are specified.

6. The novel thermoregulatory model in conjunction with user specifications for diurnal/nocturnal/crepuscular activity allows for estimates of activity time that are in good agreement with published data.

7. Climate/body size/gut model calculations for different food types suggest that optimal body size (maximizing discretionary mass/energy) changes with different food types and their associated digestive efficiencies and the temperature. This suggests that vegetation diversity in a locality allows for specific multiple body sizes to coexist at the same point in time. As food quality declines from high digestive efficiencies of flesh/seeds to lower digestive efficiencies of grasses/leaves, optimal body size increases, lowest survival temperature rises, and the degree of clumping predicted for species in nature declines. Land use changes that tend toward monocultures would appear to dictate that fewer species would survive as vegetation diversity declines. Global warming trends would lead to smaller optimal body sizes with no change in vegetation. However vegetation changes associated with climate warming would specify larger or smaller body sizes depending on whether vegetation digestive qualities decrease or increase respectively.

8. Application of the microclimate and endotherm models to rare or endangered species requires relatively few, easily measured data to estimate food and water requirements, potential for activity time, growth, and reproduction for a wide variety of habits. This information will be useful as an aid for identification of potential reserves/transplantation sites and modification/management of existing habitats.

ACKNOWLEDGMENTS

This work was supported in part by a sabbatical fellowship to the senior author by the National Center for Ecological Analysis and Synthesis and by sabbatical support from the University of Wisconsin, Madison. We thank Dr. Paul Maderson and Dr. Dominique Homberger, symposium organizers, for the invitation to the symposium and for their meticulous editing and thoughtful comments on the manuscript. We thank Dr. Joel Brown, Dr. Jordi Bascompte, and two anonymous reviewers for many thoughtful, helpful comments on the manuscript. We thank Dr. Teresa Bucher for helpful information on birds and their metabolic measurements. We thank Dr. Mark Cook and Dr. William Karasov for information on digestion and gut function. We thank Dr. Mark Burgman, Brendan Wintle, Debra McDonald, and Peter Menkhorst for specimens and data on the Orange-bellied Parrot. We thank Dick Dwelle for parrot solar reflectance measurements and feather depth measurements on museum specimens

of the Orange-bellied parrot and the peach-faced lovebird.

REFERENCES

Adolph, S. C. and W. P. Porter. 1993. Temperature, activity, and lizard life histories. Am. Nat. 142: 273–295.

Adolph, S. C. and W. P. Porter. 1996. Growth, seasonality, and lizard life histories: Age and size at maturity. Oikos 77:267–278.

Bakken, G. S. 1991. Wind speed dependence of the overall thermal conductance of fur and feather insulation. J. Therm. Biol. 16:121–126.

Bakken, G. S. and K. E. Lee. 1992. Effects of wind and illumination on behavior and metabolic rate of American goldfinches (*Carduelis tristis*). Auk 109:119–125.

Bakken, G. S., M. T. Murphy, and D. J. Erskine. 1991. The effect of wind and air temperature on metabolism and evaporative water loss rates of dark-eyed juncos, *Junco hyemalis*: A standard operative temperature scale. Physiol. Zool. 64:1023–1050.

Bartlett, P. N. and D. M. Gates. 1967. The energy budget of a lizard on a tree trunk. Ecology 48:315–322.

Beckman, W. A., J. W. Mitchell, and W. P. Porter. 1971. Thermal model for prediction of a desert iguana's daily and seasonal behavior. Trans. ASME Paper No. 71-WA/HT- 35:1–7.

Benedict, F. G. 1938. Vital energetics: A study in comparative basal metabolism. Carnegie Institute of Washington 503:133–164.

Berris, L. B. 1998. Habitat selection in time and space: The foraging ecology of raccoons. In *Department of Biological Sciences*. University of Illinois, Chicago.

Bird, R. B., W. E. Stewart, and E. N. Lightfoot. 1960. *Transport phenomena*. Wiley and Sons, Inc., New York.

Burington, R. S. 1957. *Handbook of mathematical tables*. Handbook Publishers, Inc., Sandusky, Ohio.

Brown, J. H., P. A. Marquet, and M. L. Taper. 1993. Evolution of body size: Consequences of an energetic definition of fitness. Am. Nat. 142:573–584.

Brown, J. H. and B. A. Maurer. 1987. Evolution of species assemblages: Effects of energetic constraints and species dynamics on the diversification of the North American avifauna. Am. Nat. 130:1–17.

Brown, J. H. and P. F. Nicoletto. 1991. Spatial scaling of species composition: Body masses of North American land mammals. Am. Nat. 138:1478–1512.

Brown, J. S., B. P. Kotler, and T. J. Valone. 1994. Foraging under predation: A comparison of energetic and predation costs in a Negev and Sonoran desert rodent community. Austral. J. Zool. 42:435–448.

Brown, J. S., B. P. Kotler, and W. A. Mitchell. 1997. Competition between birds and mammals: A comparison of giving-up densities between crested larks and gerbils. Evol. Ecol. 11(6):757–771.

Bucher, T. L. 1983. Parrot eggs, embryos and nestlings: Patterns and energetics of growth and development. Physiol. Zool. 56:465–483.

Bucher, T. L., G. A. Bartholomew, W. Z. Trivelpiece, and N. J. Volkmann. 1986. Metabolism, growth, and activity in Adelie (Pygoscelis adeliae) and emperor penguin (Aptenodytes forsteri) embryos. Auk 103:485–493.

Bucher, T. L. and K. R. Morgan. 1989. The effect of ambient temperature on the relationship between ventilation and metabolism in a small parrott (*Agapornis roseicollis*). J. Comp. Physiol. B 159: 561–567.

Budaraju, S., W. E. Stewart, and W. P. Porter. 1994. Prediction of forced ventilation in animal fur from a measured pressure distribution. Proc. Roy. Soc. London B 256:41–46.

Budaraju, S., W. E. Stewart, and W. P. Porter. 1997. Mixed convective heat and moisture transfer from a horizontal furry cylinder in transverse flow. Int. J. Heat and Mass Transfer 40:2273–2281.

Calder, W. A. I. 1984. *Size, function, and life history*. Harvard University Press, Cambridge.

Christian, K., C. R. Tracy, and W. P. Porter. 1983. Seasonal shifts in body temperature and use of microhabitats by Galapagos (Ecuador) land iguanas (*Conolophus pallidus*). Ecology 64:463–468.

Conley, K. E. and W. P. Porter. 1986. Heat loss from deer mice (*Peromyscus*): Evaluation of seasonal limits to thermoregulation. J. Exp. Biol. 126:249–269.

Drechsler, M., M. A. Burgman, and P. W. Menkhorst. 1998. Uncertainty in population dynamics and its consequences for the management of the orange-bellied parrot *Neophema chrysogaster*. Biol. Cons. 84:269–281.

Enquist, B. J., J. H. Brown, and G. B. West. 1998. Allometric scaling of plant energetics and population density. Nature 395:163–165.

Frost, T. M., S. R. Carpenter, A. R. Ives, and T. K. Kratz, 1994. *In* C. G. Jones and J. H. Lawton (eds.), *Linking species and ecosystems*, pp. 224–239. Chapman and Hall, New York.

Grant, B. W. and W. P. Porter. 1992. Modeling global macroclimatic constraints on ectotherm energy budgets. Am. Zool. 32:154–178.

Guyton, A. C. 1991. *Textbook of medical physiology*. 8th ed. W.B. Saunders, Philadelphia.

Hainsworth, F. R. 1981. *Animal physiology*. Addison-Wesley Publishing Co., Reading, MA.

Hayes, S. R. and J. A. Gessaman. 1980. The combined effects of air temperature, wind and radiation on the resting metabolism of avian raptors. J. Therm. Biol. 5:119–126.

Hayes, S. R. and J. A. Gessaman. 1982. Prediction of raptor resting metabolism: Comparison of measured values with statistical and biophysical estimates. J. Therm. Biol. 7:45–50.

Holling, C. S. 1992. Cross-scale morphology, geometry, and dynamics of ecosystems. Ecol. Monog. 62:447–502.

Hutchins, B. R. and R. H. Lovell. 1982. Australian parrots: Aviculture and their habits: Orange-bellied parrot *Neophema chrysogaster* (Latham). Austral. Avicult. January:11–16.

Hutchinson, G. E. 1959. Homage to Santa Rosalia, or why are they are so many kinds of animals? Amer. Nat. 93:145–159.

Kelrick, M. R. and J. A. MacMahon. 1985. Nutritional and physical attributes of seeds of some common sagebrush-steppe plants: Some implications for ecological theory and management. J. Range Manage. 38(1):65–69.

Kenagy, G. J., R. D. Stevenson, and D. Masman. 1989. Energy requirements for lactation and postnatal growth in captive golden mantled ground squirrels. Physiol. Zool. 62:470–487.

Kingsolver, J. G. 1979. Thermal and hydric aspects of environmental heterogeneity in the pitcher plant mosquito (*Wyeomyia smithii*). Ecol. Monog. 49: 357–376.

Kleiber, M. 1975. *The fire of life. An introduction to animal energetics.* 2nd ed. Krieger Publishing Co., Huntington, New York.

Kowalski, G. J. and J. W. Mitchell. 1976. Heat transfer from spheres in the naturally turbulent, outdoor environment. J. Heat Transfer 98(4):649–653.

Kowalski, G. J. 1978. An analytical and experimental investigation of the heat loss through animal fur. In *Department of Mechanical Engineering.* University of Wisconsin, Madison, Wisconsin.

Lawton, J. H. and V. K. Brown. 1993. *In* E. D. Shultz and H. A. Mooney (eds.), *Biodiversity and ecosystem function*, pp. 255–270. Springer-Verlag, Berlin.

Lide, D. R. and H. P. R. Frederikse. (eds.) 1996. *CRC handbook of chemistry and physics. A ready-reference book of chemical and physical data.* CRC Press, Orlando.

Levey, D. J. and W. A. Karasov. 1992. Digestive modulation in a seasonal frugivore, the American robin (*Turdus migratorius*). Am. J. Physiol. 262(4 Part 1):G711–G718.

Loyn, R. H., B. A. Lane, C. Chandler, and G. W. Carr. 1986. Ecology of orange-bellied parrots *Neophema chrysogaster* at their main remnant wintering site. The Emu 86:195–206.

MacArthur, R. E., H. Recher, and M. Cody. 1966. On the relation between habitat selection and species diversity. Am. Nat. 100:319–332.

Mathieu, O., R. Krauer, H. Hoppeler, P. Gehr, S. L. Lindstedt, R. M. Alexander, C. R. Taylor, and E. R. Weibel. 1981. Design of the mammalian respiratory system: 7. Scaling mitochondrial volume in skeletal muscle to body mass. Resp. Physiol. 44: 113–128.

Maurer, B. A., J. H. Brown, and R. D. Rusler. 1992. The micro and macro in body size evolution. Evolution 46:939–953.

McClure, P. A. and W. P. Porter. 1983. Development of insulation in neonatal cotton rats (*Sigmodon hispidus*). Physiol. Zool. 56:18–32.

McCullough, E. M. and W. P. Porter. 1971. Computing clear day solar spectra for the terrestrial ecological environment. Ecology 52:1008–1015.

McNaughton, S. J. 1977. Diversity and stability of ecological communities: A comment on the role of empiricism in ecology Am. Nat. 111:515–525.

McNaughton, S. J. 1985. Ecology of a grazing ecosystem: The Serengeti (Tanzania, Kenya). Ecol. Monogr. 55(3):259–294.

Mitchell, J. W. and G. E. Myers. 1968. And analytical model of the counter-current heat exchange phenomena. Biophys. J. 8(8):897–911.

Mitchell, J. W. 1976. Heat transfer from spheres and other animal forms. Biophys. J. 16:561–569.

Mitchell, J. W., W. A. Beckman, R. T. Bailey, and W. P. Porter. (eds.) 1975. *Microclimatic modeling of the desert*, pp. 275–286. Scripta Book Co., Washington D.C.

Morris, J. G. and S. C. Kendeigh. 1981. Energetics of the prairie deer mouse, Peromyscus maniculatus bairdii. Am. Mid. Nat. 105:368–376.

Morrison, P. R. 1960. Some interrelations between weight and hibernation functions Bull. Mus. Comp. Zool. Harvard U. 124:75–91.

Norris, K. S. 1967. Color adaptation in desert reptiles and its thermal relationships. *In Symposium on lizard ecology*, pp. 162–229. University of Missouri Press, Columbia Missouri.

Penry, D. L. and P. A. Jumars. 1987. Modeling animal guts as chemical reactors. Am. Nat. 129:69–96.

Peterson, C. C., K. A. Nagy, and J. Diamond. 1990. Sustained metabolic scope. PNAS v. 87(6):2324–2328.

Peterson, G., R. Allen Craig, and C. S. Holling. 1998. Ecological resilience, biodiversity, and scale. Ecosystems, Jan. Feb. 1:6–18.

Porter, W. P. and D. M. Gates. 1969. Thermodynamic equilibria of animals with environment. Ecol. Monog. 39:227–244.

Porter, W. P. and F. C. James. 1979. Behavioral implications of mechanistic ecology II: The African rainbow lizard, *Agama agama* Copeia 1979(4): 594–619.

Porter, W. P., J. W. Mitchell, W. A. Beckman, and C. B. DeWitt. 1973. Behavioral implications of mechanistic ecology: Thermal and behavioral modeling of desert ectotherms and their microenvironment. Oecologia 13:1–54.

Porter, W. P., J. C. Munger, W. E. Stewart, S. Budaraju, and J. Jaeger. 1994. Endotherm energetics: From a scalable individual-based model to ecological applications. Austral. J. Zool. 42:125–162.

Press, W. H., B. P. Flannery, S. A. Teukolsky, and W. T. Vetterling. 1986. *Numerical recipes. The art of scientific computing.* Cambridge University Press, Cambridge.

Rogowitz, G. L. and J. A. Gessaman. 1990. Influence of air temperature, wind and irradiance on metabolism of white-tailed jackrabbits. J. Therm. Biol. 15:125–132.

Roughgarden, J. 1974. Niche width: Biogeographic patterns among Anolis lizard populations. Amer. Nat. 108:422–442.

Schmidt-Nielsen, K. 1979. *Animal physiology. Adaptation and environment.* 2nd ed. Cambridge University Press, Cambridge.

Scholander, P. F. 1940. Experimental investigations on the respiratory function in diving mammals and birds. Hvalradets Skrifter 22:1–131.

Scholander, P. F., R. Hock, V. Walters, S. Johnson, and L. Bruibs. 1950. Heat regulation in some arctic

and tropical mammals and birds. Biol. Bull. Woods Hole 99:237–258.
Siemann, E. and J. H. Brown. 1999. Gaps in mammalian body size distributions reexamined. Ecology 88(8):2788–2792.
Steudel, K., W. P. Porter, and D. Sher. 1994. The biophysics of Bergmann's rule: A comparison of the effects of pelage and body size variation on metabolic rate. Can. J. Zool. 72:70–77.
Stewart, W. E., S. Budaraju, W. P. Porter, and J. Jaeger. 1993. Prediction of forced ventilation in animal fur under ideal pressure distribution. Functional Ecology 7:487–492.
Taylor, C. R., N. C. Heglund, and G. M. O. Maloiy. 1982. Energetics and mechanics of terrestrial locomotion: 1. Metabolic energy consumption as a function of speed and body size in birds and mammals. J. Exp. Biol. 97:1–22.
Tilman, D. and J. A. Downing. 1994. Biodiversity and stability in grasslands. Nature 367(6461):363–365.
Waldschmidt, S. R., S. Jones, and W. P. Porter. 1987. Reptilia. *In* Pandian (ed.), *Animal energetics* Bivalvia *through* Reptilia, Vol. 2, pp. 553–619. Academic Press, San Diego.
Walsberg, G. E. 1988*a*. The significance of fur structure for solar heat gain in the rock squirrel, *Spermophilus variegatus*. J. Exp. Biol. 138:243–258.
Walsberg, G. E. 1988*b*. Heat flow through avian plumages: The relative importance of conduction, convection and radiation. J. Therm. Biol. 13:89–92.
Walsberg, G. E. 1988*c*. Consequences of skin color and fur properties for solar heat gain and UV irradiance in two mammals. J. Comp. Physiol. B Biochem. System. Environ. Physiol. 158:213–222.
Walsberg, G. E. and B. O. Wolf. 1995. Solar heat gain in a desert rodent: Unexpected increases with wind speed and implications for estimating the heat balance of free-living animals. J. Comp. Physiol. B Biochem. System. Environ. Physiol. 165: 306–314.
Wathen, P., J. W. Mitchell, and W. P. Porter. 1971. Theoretical and experimental studies of energy exchange from jack rabbit ears and cylindrically shaped appendages. Biophys. J. 11(12):1030–1047.
Wathen, P. M., J. W. Mitchell, and W. P. Porter. 1974. Heat transfer from animal appendage shapes-cylinders, arcs, and cones. Trans. of the ASME. November. 40:536–540.
Weibel, E. R., C. R. Taylor, and H. Hoppeler. 1991. The concept of symmorphosis: A testable hypothesis of structure–function relationship. Proc. Nat. Acad. Sci. USA. 88:10357–10361.
Weiner, J. 1987. Limits to energy budget and tactics in energy investments during reproduction in the Djungarian hamster (*Phodopus sungorus sungorus*) Pallas 1770. In *Reproductive energetics in mammals.* Symp. Zool. Soc. London 57:167–187.
Welch, W. R. and C. R. Tracy. 1977. Respiratory water loss: A predictive model. J. Theor. Biol. 65:253–265.
Welch, W. R. 1980. Evaporative water loss from endotherms in thermally and hygrically complex environments: An empirical approach for interspecific comparisons. J. Comp. Physiol. (B) 139:135–143.
West, G., J. H. Brown, and B. J. Enquist. 1997. A general model for the origin of allometric scaling laws in biology. Science 276:122–126.
West, G., J. H. Brown, and B. J. Enquist. 1999. The fourth dimension of life; fractal geometry and allometric scaling of organisms. Ecology (In press).

ABBREVIATIONS

Symbols

T = temperature (C, K)
m = mass (kg)
Q = heat flux (W)
R, r = radius (m)
RH = relative humidity (%)
V = wind speed (m/s)
Subscripts
abs = absorbed
air = free stream air
cond = conduction
evap = evaporation
f = fur
grd = ground
IR = infrared
met = metabolism
opt = optimal
resp = respiration
s = skin

APPENDIX

Allometry model

Equations used for calculating allometry of large birds were derived from their weight and photographs. All units are SI (m, kg, W). Equations used for allometry of large birds are for the size range: Rhea (25 kg) to Ostrich (100 kg):

Body feathered length (top of head to base of tail) (m) = 0.225 mass $(kg)^{0.312}$

Bare portion of leg only; feathered leg part treated as part of the body

$$\text{Leg length (m)} = L(\text{leg}) = 0.00613[\text{mass(kg)} - 25.] + 0.61$$

$$\text{Leg diameter (m)} = D(\text{leg}) = 0.000453[\text{mass(kg)} - 25.] + 0.057$$

$$\text{Area of one leg} = A(\text{leg}) = \pi D(\text{leg})L(\text{leg})$$

$$\text{Volume of one leg} = \pi(D(\text{leg})/2.)^2 L(\text{leg})$$

Head/neck (assuming no feathers for the rattites)

Head plus neck length (m)

$$= 0.00253[\text{mass(kg)} - 25.] + 0.57$$

Head and neck diameter (m)

$$= 0.0000507[\text{mass(kg)} - 25.] + 0.0572$$

Area of neck/head

$$= \pi D(\text{neck})L(\text{head\&neck})$$

Volume of Head & neck

$$= \pi(D(\text{neck})/2)^2 L(\text{head\&neck})$$

Total volume(m^3)

$$= \text{mass(kg)}/1000(\text{kg}/m^3)$$

Torso volume

= Total volume − Leg volume

− Head&neck volume

Estimating average feather depth of rattite birds from photographs and weights.

Estimating feather–air surface area for calculating convection from feather surface from photographs and weights.

Semi-major axes of an ellipsoid for feather–air interface of rattites

$$a = \text{long axis(m)}/2$$

$$= (-0.00227(\text{mass(kg)} - 100.) + 1.75)/2$$

$$b = \text{width(m)}/2 = (0.00173(\text{mass(kg)} - 25.) + 1.0)/2$$

$$c = \text{height(m)}/2$$

$$= (-0.00267(\text{mass(kg)} - 100.) + 1.0)/2$$

The area of a prolate ellipsoid is

$$\text{Area}(m^2) = 2\pi((b + c)/2)^2 + 2\pi(a((b + c)/2.)/e)\sin^{-1}(e)$$

where

$$e = [(a^2 - ((b + c)/2)^2)]^{0.5}/a \text{ (Burington [1957])}$$

Estimating unfeathered torso dimensions for the equation of ellipsoid heat generation needed to maintain core temperature.

We assume geometric similarity of shape (uniform feather depth) for the bare torso surface and the feather–air surface.

The volume of a prolate ellipsoid contained within the feather–air interface is

$$\text{Volume, feathered torso} = (4/3)\ \pi abc$$

Assuming the same ellipsoid shape for torso and feather–air interface.

$$\text{Volume, bare torso} = V, \text{baretorso} = (4/3)\ \pi(abc)x^3$$

where x is the common fractional factor for a, b, and c that gives the exact torso semi-major axes. We know the feathered torso volume from the equation above and the semi-major axes of the feathered torso, a, b, and c. We can solve for x, the common fractional factor for a, b, and c.

$$x = (3V,\text{baretorso}/(4\pi\ abc))^{0.3333}$$

Thus, the bare torso semi-major axes are

$$A,\text{torso} = ax \qquad B,\text{torso} = bx \qquad C,\text{torso} = cx$$

Average feather depth is the difference between any of the feathered and unfeathered semi-major axes, e.g. (a, feathered torso—A, bare torso).

The characteristic dimension for the Nusselt–Reynolds heat transfer coefficient calculation is

$$D = \text{Volume,feathered torso}^{0.3333}$$

Gut model

The goal here was to determine an *upper bound for absorbed food.* It does not explicitly consider important constraints on food intake that are affected by how food is distributed in the environment, which affects encounter probability, and what the handling time is, which is a function of feeding apparatus morphology. Both encounter probability and handling time may affect how much food is actually ingested. This version of the gut model waits until a 24 hr activity simulation cycle starting at midnight has been completed. Then it looks back at the day's energy requirements and uses that to calculate how much of the food would have to be processed in the gut that day to meet those demands.

The user specifies the food properties. They include percent of proteins, carbohydrates, lipid, and percent dry mass relative to wet mass. There is an upper bound constraint; the animal may never consume more wet weight food per day than its body mass.

The gut model deals only with the part of the gut associated with the actual digestive process. Handling time and internal storage of food in the stomach(s) is not considered. These will place additional constraints on gut function. Because retention time may vary from approximately one-third of a day to more than a day, depending on body size, it was finally decided to use a day's energy requirements and the mass flow of food per day needed to meet those requirements. In all these simulations the assumption was made that the total energy requirements were 3.5 times the energy needed to maintain core temperature on the particular day that was simulated.

A digestive efficiency of 57% was used for most of the simulations, except for grass hay, Reference No. 102250 (U.S.–Canadian nutrient composition tables, 1994). A 57% digestive efficiency has been measured for seeds in small rodents and is very close to the value for digestive efficiency by cattle (61%). The model requires empirical data on digestive efficiency, food properties defined above. The gut model assumes that the gut can alter flow rates to maintain the same digestive efficiency for a particular type of food (Levey and Karasov, 1992).

Animals typically do not overeat or gain weight unnecessarily. The model assumes that the amount of food ingested is determined by today's metabolic needs and is constrained by maximum volumetric flow rate less than or equal to body mass. The user defines percent digestive efficiency, percent water in feces, percent urea in urine, and a multiplier from 1 to 7 above basal metabolic energy requirements to specify food intake to meet current needs. The user also defines percent protein, percent fat, percent carbohydrate, and percent dry matter in ingested food.

The dry grams of food needed to meet the metabolic demand are estimated based on food properties and the constraints in the paragraph above.

The gut model is related to work by Penry and Jumars (1987). Their equation (9), p. 73, for a batch reactor model is

$$\text{time} = C_{A_0} \int_0^{X_{af}} (dX_A / - r_A)$$

where

X_A = mole fraction of species A (dimensionless)

$X_A = (C_{A_0} - C_A)/C_{A_0}$

C_A = food component, A, concentration (moles)

C_{A_0} = initial concentration of food component, A, in moles.

Many of the components of reactor models are not known. Since the endotherm model can calculate metabolic heat production to maintain a specified core temperature, it is straightforward to calculate the grams dry weight, and then wet weight of user-defined food to meet the metabolic demand. The following pseudoequations are an example of these calculations for a seed diet.

The amount of fat, protein, and carbohydrate/g dry mass of food is first computed from user specified percentages of these components of food.

gfatpg = pctfat(g fat/g dry mass)

gprotpg = pctpro(g protein/g dry mass)

gcarbpg = pctcar(g digestible carbohydrate/g dry mass)

gsum = gfatpg + gprotph + gcarbpg

Next undigested mass/g dry mass of food is calculated and used to compute total carbohydrates.

gundig = 1.00 − gsum

TOTCARB = gcarbpg + gundig

Then joules/g dry food is calculated

fatJpg = gfatpg × (9400 × 4.185)
× (g fat/g dry food × calories/g fat
× J/calorie)

protJpg = gprotpg × (4199 × 4.185)

carbJpg = TOTCARB × (4200. × 4.185)

TotJpgram = fatJpg + protJpg + carbJpg

Not implemented here is the variable protein digestion efficiency for ruminants vs. monogasters (~75% *vs.* 13%). While proteins are important from a protein and amino acid balance standpoint, in terms of absolute energy available, it is a small factor, since alfalfa (reference number 100056) *vs.* grass forage (reference number 102250) varies from approximately 8.6% protein to 18.1% protein (U.S.–Canadian nutrient compound composition tables, 1994). Seed protein is 15% (Kelrick and MacMahon, 1985). Calculation of joules absorbed per gram of dry food is:

Jabspgr = fatJpg + protJpg + DigEff × carbJpg

The moles available/g dry food can now be calculated.

Totmolpgram = gfatpg × 850. + gprotpg × 137
+ gcarbpg × 180.

We can then calculate the joules of chemical energy needed to be absorbed by the gut /day = (J/s) × (s/h) × 24h × basal multiplier for metabolic rate (activity above resting)

FoodJ = Qmetab × 3600. × 24. × timbas

The dry mass needed to be absorbed/d to meet the metabolic demand is then

DRYABS = FoodJ/Jabspgr

We then calculate the grams of dry food that must be ingested/day and then the total moles of each of the foodstuffs

Drymas = DRYABS/(1.0 − gundigest)

Total moles available for absorption = moles/dry gram × dry grams

Totmoles = (gfatpg × 850. + gprotpg × 137
+ gcarbpg × 180.) × drymas

The J of food needed in gut/day to meet nesting metabolism plus user specified activity level = (J/DAY) × basal multiplier

FoodJ = DaysMETAB × timbas

The needed g of food absorbed/d = J needed/day/Food J/g

DRYABS = FoodJ/Jabspgr

The g food dry ingested/day = g absorb/Digest_Efficiency

Drymas = DRYABS/(1.0 − gundiest)

Wetmas = Drymas/PctDry

We then test for whether the required food mass per day exceeds body mass. If it does, absorbed mass is reset to the maximum value allowed by body weight and energy available is adjusted accordingly.

Upprlim = Gmass

If (Wetmas .greaterthan. Upprlim) then

Wetmas = Upprlim

Drymas = Wetmas × PctDry

DRYABS = Drymas × Digest_Efficiency

Jpdaymax = DRYABS/Jabspgr

Jpsavail = Jpdaymax/(24. × 3600.)

Endif

Once we have checked to make sure the upper bound has not been exceeded, the day's joules of energy absorbed, DaysJabs, can be calculated.

$$\text{DaysJabs} = \text{Jabspgr}*\text{DRYABS}$$

The energy available, Avlnrg, in joules/sec available can be calculated

$$\text{Avlnrg} = \text{DaysJabs}/(24.*3600.)$$

We calculate the g wet weight through the gut/day, CRTOT, to monitor part of the water balance of the animal.

$$gH_2O = (\text{Drymas} - \text{PCTDRY} \times \text{Drymas})/\text{PCTDRY}$$

$$\text{CRTOT} = gH_2O + \text{Drymas}$$

We also keep track of the hourly dry grams absorbed of protein, fat and carbohydrate for use in the growth model (Adolph and Porter, 1996).

$$\text{Dryinphr} = \text{DRYABS}/24.$$

$$\text{GPROTH} = \text{Dryinphr} \times \text{gprotpg}$$

$$\text{GFATH} = \text{Dryinphr} \times \text{gfatpg}$$

$$\text{GCARBH} = \text{Dryinphr} \times \text{gcarbpg}$$

Size dependent constraints appear when the energy (mass) needs for the day exceed the daily gut volume flow rate for the body size. Available activity time available is calculated. That can be used to back calculate required handling time of the food needed to meet the energetic demands and to estimate time efficiency of mass/energy acquisition for all body sizes for a given food type and configuration.

Data sources: This model assumes 0.40 g water/g protein oxidized: Hainsworth (1981).

Proteins

Approximate gram molecular weight of amino acids is 137 g/mole

Based on information from the *CRC Handbook of Chemistry and Physics* (1996)

Alanine = 89.1 g/mole (with water − 18 g/mole)

Arginine = 174.2 g/mole (with water − 18 g/mole)

Aspargine = 132.1 g/mole (with water − 18 g/mole)

Aspartic acid = 133.1 g/mole (with water − 18 g/mole)

Cystine = 121.2 g/mole (with water − 18 g/mole)

Glutamic acid = 147.1 g/mole (with water − 18 g/mole)

Glutamine = 146.1 g/mole (with water − 18 g/mole)

Glycine = 75.1 g/mole (with water − 18 g/mole)

Histidine = 155.2 g/mole (with water − 18 g/mole)

Isoleucine = 131.2 g/mole (with water − 18 g/mole)

Leucine = 131.2 g/mole (with water − 18 g/mole)

Lysine = 146.2 g/mole (with water − 18 g/mole)

Methionine = 149.2 g/mole (with water − 18 g/mole)

Phenylalanine = 165.2 g/mole (with water − 18 g/mole)

Proline = 115.1 g/mole (with water − 18 g/mole)

Serine = 105.1 g/mole (with water − 18 g/mole)

Threonine = 119.1 g/mole (with water − 18 g/mole)

Tryptophan = 204.2 g/mole (with water − 18 g/mole)

Tyrosine = 181.2 g/mole (with water − 18 g/mole)

Valine = 117.1 g/mole (with water − 18 g/mole)

Average = 137 g/mole

Lipids

Data from Guyton (1991). The gut model assumes that triglycerides are used for energy. They are stearic acid (880 g/mol), oleic acid (879 g/mol) and palmitic acid (754 g/mol). Based on these data the model assumes as an average 850 g/mol. The model uses 4.7 calories/ml O_2 which is 9,400 calories/g fat (Kleiber, 1975). There are 1.07 g water produced/g lipid oxidized: Hainsworth (1981).

Carbohydrates

This model assumes that glucose data values are 180 g/mol; 5.0 cal/ml O_2; 4,200 calories/g (Kleiber, 1975) and that there are 0.56 g water produced/g carbohydrate oxidized: Hainsworth (1981).

Digestion capability data come from Weiner (1987), Kenagy *et al.* (1989), and Peterson *et al.* (1990). Seed component values come from Kelrick and MacMahon (1985).

The input data file for the mouse to elephant calculations is listed below. Labels above it describe each datum.

Animal species = Mouse to elephant, deer mouse fur; grass hay—Ref. #102250
ALLOMETRIC properties:

Max. weight (kg)	Min. weight (kg)	Fat insul. thick (m)	Geometric approx. (integer) 1 = cyl, 2 = spher, 3 = ellips, 4 = lizard	'Ibgird' or 'Igmaml' = >20kg, uses complex geom's	% ventral area on substrate (decimal %)
10,000	0.010	0.0	3	'Igmaml'	0.05

FUR Properties

Hair dia. (μm)		Hair length (mm)		Fur depth (mm)		Hair dens. (1/cm2)		Fur solar reflect.	Fur solar transmiss.
dsl	vntl	dsl	vntl	dsl	vnt	dsl	vntl	nd	nd
30.	30.	9.	9.	6.6	6.6	12,000.	12,000.	0.2	0.14

PHYSIOLOGICAL properties—temperature and water loss from metabolism & skin

Core temp.	Min. diff Tc-Tskin (C)	Texpir-Tair (C)	% skin wet (sweat)	Thermal conductivity of flesh (0.412–2.8 W/mC)
36.0	0.5	3.0	1.	0.9

PHYSIOLOGICAL properties—gut and excretory system

Digest. eff. (dec. %)	Fecal water (dec. %)	Urea in urine (dec. %)	X basal metabolism (W) for est. food intake (1.5–7)
0.61	0.10	0.20	3.5

FOOD properties

% protein (decimal)	% fat (decimal)	% carbohydrate (decimal)	% dry matter (decimal) (0.25 green veg.; 0.75 seed humid stor.; 0.9219 dry seed)
0.086	0.023	0.42	0.25

BEHAVIORAL data:

Diurnal? (Y/N)	Burrow? (Y/N)	Climb to Cool OK? (Y/N)	Ground shade seeking OK? (Y/N)	Crepuscular activity? (Y/N)	Fossorial only)? (Y/N)
'n'	'n'	'n'	'n'	'n'	'n'

NEST properties: if nest thickness = 0.0 & thermal cond. = 0.0, no nest assumed

Nest wall thickness (m)	Nest wall thermal conductivity (W/m-C)
0.00	0.0

A sample input data file for the microclimate model is listed below to illustrate the data required for microclimate calculations. The format is like that for the endotherm model listed above. Animal height is average height to the middle of the body. This allows for calculation and output of the air temperature and wind speed at average animal height for outdoor calculations.

Site Label

Savannah River Site, Aiken County, South Carolina

Roughness height (m)	Soil therm. cond. (W/mC)	Sub. refl. (dec%)	Sub. dens. (kg/m3)	Sub. specific heat (J/m3-K)	Sub. longIR emiss (dec%)	Integrator error	Animal ave. height (cm)
0.001	2.5	0.30	2,650	837.	0.90	2.	5.

Start month #	End month #	Percent of bare ground in shade (0% = full sun)
1	12	0

Hemisphere N = 1, S = 2	Latitude (deg)	Latitude (min)	W Longitude (deg)	W Longitude (min)	15 × integer Longit. time zone (deg)	Slope (deg)	Azimuth (S = 0 (deg)	Elev. (m)	Cm H_2O in air col.
1.0	33.0	24.0	81.0	39.0	75.0	10.0	0.0	0.0	1.5

Time of MAXIMUMS (top row), Minimums (bottom row): Air, Wind max's ~ solar noon (integer hours relative to sunrise or solar noon) Rel. Hum, Clouds max's ~ sunrise

Air temp.	Wind speed	Rel. hum.	Cloud cover
1.0	1.0	0.0	0.0
0.0	0.0	1.0	1.0

Max's (top row), min's (bottom row) REL HUMIDITIES (%) for ave. day each month

83.0	82.0	84.0	85.0	86.5	86.5	88.5	92.0	92.0	91.0	89.0	84.5
55.0	49.5	47.5	44.0	48.5	51.5	54.5	56.5	55.5	50.5	51.0	53.0

Max's (top row), min's (bottom row) CLOUD COVER (%) for ave. day each month

0.	0.	0.	0.	0.	0.	0.	0.	0.	0.	0.	0.
0.	0.	0.	0.	0.	0.	0.	0.	0.	0.	0.	0.

Max's (top row), min's (bottom row) WIND SPEED (m/s) for ave. day each month

2.5	2.5	2.5	2.5	2.5	2.5	2.5	2.5	2.5	2.5	2.5	2.5
0.5	0.5	0.5	0.5	0.5	0.5	0.5	0.5	0.5	0.5	0.5	0.5

Max's (top row), min's (bottom row) AIR TEMPERATURE (C) for ave. day each month

14.3	17.5	22.0	26.9	30.2	33.4	35.2	33.2	30.8	25.4	21.1	15.4
0.5	2.6	5.6	8.9	14.0	18.8	21.2	20.5	16.8	9.9	5.8	0.8

The executable code and data for input to the program for these calculations are available from the senior author to interested readers. Questions about code details should be directed to the senior author.